Implementation of Active Membrane Noise Absorber in Duct Based on Fuzzy Model Control Strategy

Department of Electrical Power Engineering and Mechatronics

Master Thesis

Supervisor:

Prof.Trieu Minh Vu

Student:

Reza Moezzi 147286

2017

AUTHOR'S DECLARATION

Hereby I declare, that I have written this thesis independently.

No academic degree has been applied for based on this material.

All the works, major viewpoints and data of the other authors used in this thesis have been referenced.

The thesis was completed under the supervision of **Prof. Trieu Minh Vu**.

"......"……………2017

Author: Reza Moezzi

………………………..

 /signature/

The thesis complies with the requirements for graduation thesis.

"......"……………2017

Supervisor: **Prof. Trieu Minh Vu**

………………………..

 /signature/

Accepted for defence

 "......"……………2017

Chairman of ……………………… thesses' defence commission:…………………………

 /signature/

Ventilatsioonitoru membraanikujuline aktiiv-mürasummutaja hägusloogika mudeli baasil

MAGISTRITÖÖ

MEHHATROONIKA ÕPPEKAVA

Juhendaja Prof. Trieu Minh Vu

Üliõpilane Reza Moezzi

Üliõpilaskood   147286MAHM

Tallinn, 2017

AUTORIDEKLARATSIOON

Deklareerin, et käesolev lõputöö on minu iseseisva töö tulemus.

Esitatud materjalide põhjal ei ole varem akadeemilist kraadi taotletud.

Lõputöös kasutatud kõik teiste autorite tööd ja seisukohad ning materjalid on varustatud vastavate viidetega.

*Töö valmis **Prof. Trieu Minh Vu** juhendamisel*

"......"……………2017

Töö autor: Reza Moezzi

………………………..

 /allkiri/

Töö vastab lõputööle esitatavatele nõutele

"......"……………2017

*Juhendaja: **Prof. Trieu Minh Vu***

………………………..

 /allkiri/

Lubatud kaitsmisele

……………………….. õppekava lõputööde kaitsmiskomisjoni esimees: …….……………

          /allkiri/

SISUKORD / CONTETS

Table of Figures and Table

INTRODUCTION

Pipelines, intake and exhaust systems for reciprocating internal combustion engines, as well as industrial exhaust stacks are all examples of duct system in which noise generation and propagation can occur. The details of this noise propagation is important due to its potential environmental impact. Consequently, in order to reduce or optimize the level of noise, several proposals and methodologies have been proposed (Finn Jacobsen, 2009). For several years, researchers have investigated about using resonators, porous material and membrane absorbers (Finn Jacobsen, 2009). The low frequency ranges (<500) that is critical field to manage the noise level, membrane absorber has shown more convenient result (R. Bellet, 2010) but still a total passive membrane is insufficient and an active one is required and essential to comprehensive deal with noise controlling system in low frequency ranges.

MOTIVATION

Accordingly, in order to relief membrane at both the design and problem solution stage it is important to consider (i) the effect of tension on membrane surface, and (ii) how to vary the tension based on frequency range to optimize sound absorption coefficient. As a result, it is essential that we gather specific experimental information of the effect of tension on the acoustic characteristics as well as absorption coefficient in our duct system experiment.

On the other hand intelligent controllers enable us to move on from passive concepts to active field that aid to achieve desired consequences. This controller tries to adjust tension of membrane's surface based on incident wave frequency.
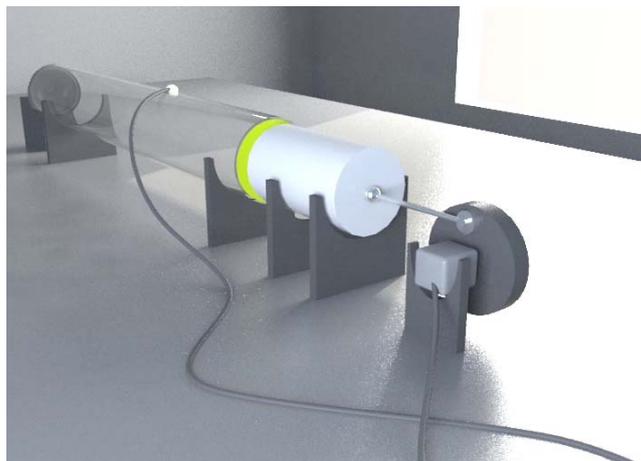
Figure 1: The system under investigation
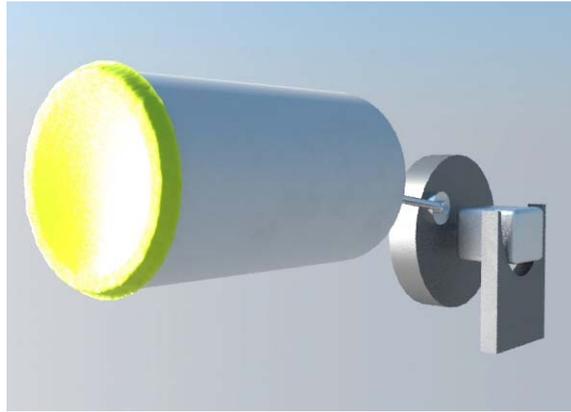
Figure 2: producing Tension on membrane surface using active exert stress

BACKGROUND

To overview the background of work, these previous literatures has been studied and considered.

As the acoustical point of view, T. E. Vigranproposed 'Measuring the Acoustic Properties of Ducts' (Vigran, 1984).In 1990 W. Frommhold and his colleagues published paper as 'Acoustic performance of Membrane absorber' (Frommhold, 1990) and discussed about the acoustic properties of absorbing elements. W. A. Thomas, Jr. and C. J. Hurst had investigated about 'Acoustic performance of a stretched membrane' (W. A. Thomas, 1975). M.H. Zainulabidin and others practically showed the effect of membrane's surface tension on sound absorption characteristics in different frequency ranges. (M.H. Zainulabidin, 2012)

Alternatively as Active noise control aspects background, SeppoUosukainen has shown the 'PanPhonics Panels in Active Control of Sound' and reviewed the active control of sound and its application (Uosukainen). In 2001 C.A. Silva, J.M. Sousa and J.M.G. S´a da Costa briefly worked on a new approach to acoustic noise control, by introducing a fuzzy controller, but in a different application (C.A. Silva, 2001). M. O. TOKHI investigated about different intelligent methods for active noise and vibration control (TOKHI, 2004) and finally M. D. Redel-Macías and his friends published a paper under title 'A novel design strategy for iterative learning controlbased on approximate fuzzy data model (AFDM) for activenoise control: Theoretical background' which just explored about the mathematical overview of problem (M. D. Redel-Macías, 2014).

METHODOLOGY

The required methodologies in this thesis are combination of different approaches from multidisciplinary science.

In order to analyse the acoustical characteristics, the Duct acoustics methodologies should be considered. Sound wave can only propagate freely in one direction. It is confined in other dimensions by duct walls.The sound wave propagation has assumed as planer wave.
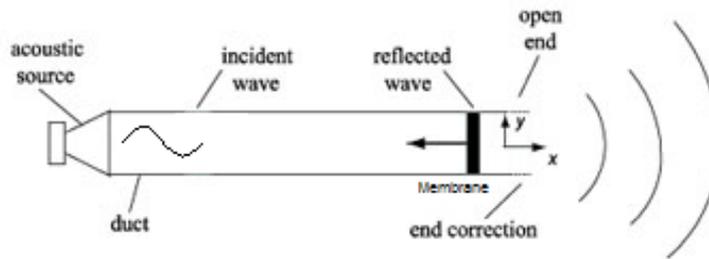
Figure 3: Duct Acoustics

In active part control system the Fuzzy approach has been deliberated. fuzzy systems are knowledge-based or rule-based systems that contain descriptive IF-THEN rules that are created from human knowledge. Two approaches could be investigated as Mamdani and Sugeno interfaces.
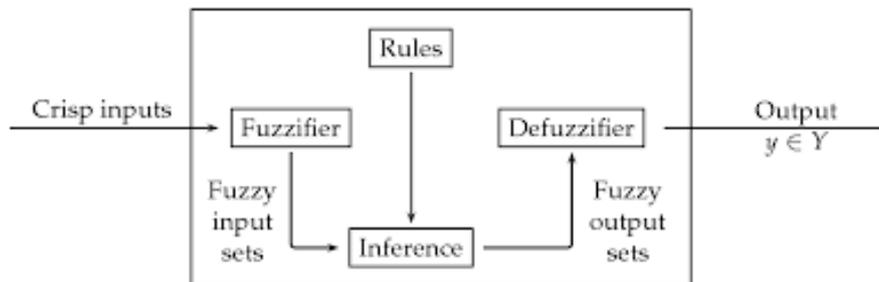
Figure 4:Fuzzy logic Algorithm

To approach to the discussed problem I've divided up the project in following steps:
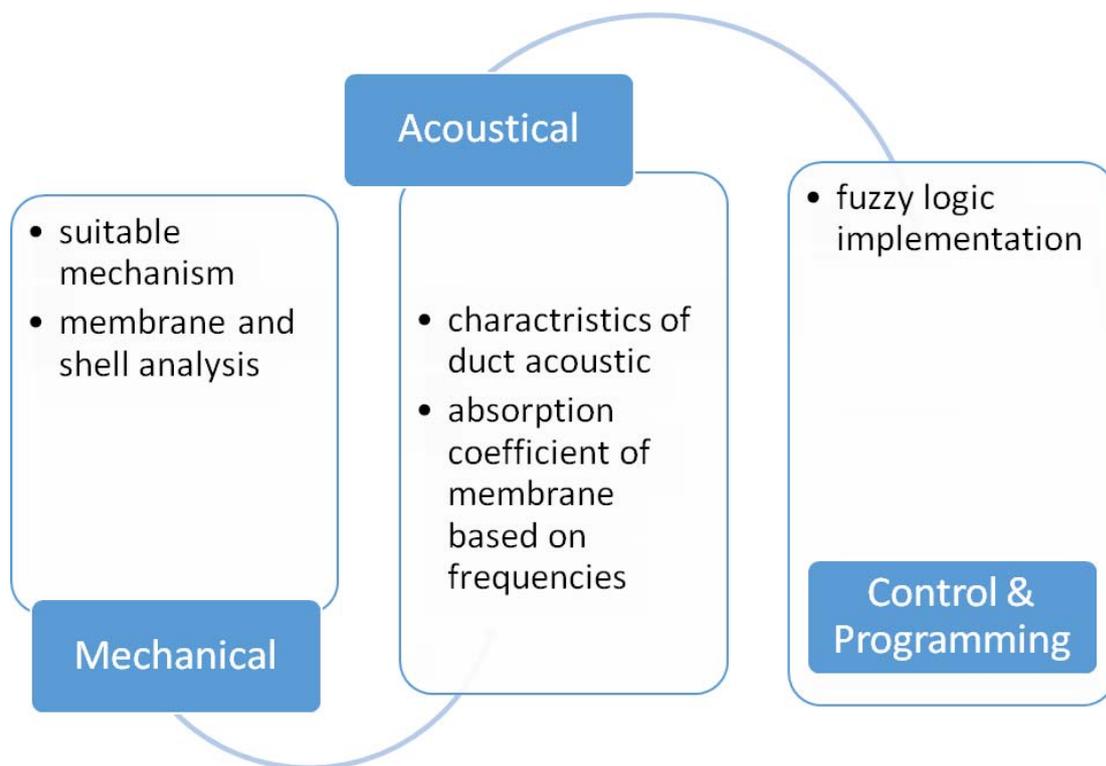
Figure 5:Steps

Mechanical:

1.1. Mechanism

Mechanisms are used in variety of fixed motion generation applications in Engineering. Among that **slider crank mechanism** is most useful mechanism today's application for numerous applications such as robotics, pumps and compressors.

A Slider Crank Mechanism is a modification of four bar chain. It consists of one sliding pair and two turning pairs. It is usually found in Reciprocating engine mechanism. This type of mechanism converts rotary motion into reciprocating motion and vice versa. However when it is used as an automobile engine by adding valve mechanism etc., it becomes a machine which converts the available energy (force on the piston) into the desired energy (torque of the Crank shaft). The torque is used to move a vehicle.

For our application also this mechanism has been considered to convert the rotary motion of servo motor to reciprocating motion of slider to exert desired force on membrane surface to stretch it to optimize the acoustical properties.This mechanism is consist of rotation, rotation& translation (RRT)
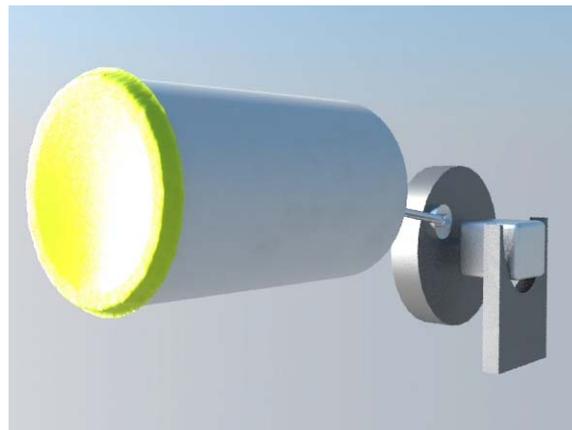
Figure 6:Mechanism
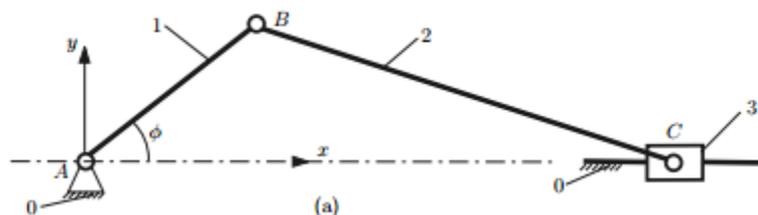
Figure 7:Mechanism diagram

1.2. Position Analysis:

First I've analyzed the position of slider (Point C) based on phi

For our application we supposed the AB (Radius of Crank) =6 Cm, the connecting rod BC =15

The driver link 1 makes an angle $\varphi \circ$ with the horizontal axis and the positions of the joints and the angles of the links with the horizontal axis could be calculated with:

Position of Joint A: A Cartesian reference frame xOy is selected. The joint A is in the origin of the reference frame, that is, $A \equiv O$, $x_A = 0$, $y_A = 0$,

Position of Joint B: The unknowns are the coordinates of the joint B, x_B and y_B. Because the joint A is fixed and the angle φ is known, the coordinates of the joint B are computed from the following expressions:

$x_B = AB \cos\varphi = (0.06) \cos \varphi\circ$ (cm)   and $y_B = AB \sin\varphi = (0.06) \sin \varphi\circ$(cm).

The MATLAB commands for above are: x_B=AB*cos(phi); y_B=AB*Sin(phi);

where phi is the angle φ in radians

Position of Joint C: The unknowns are the coordinates of the joint C, x_C and y_C. The joint C is located on the horizontal axis $y_C = 0$

The length of the segment BC is constant $(x_B - x_C)^2 + (y_B - y_C)^2 = BC^2$

or $((0.06) \cos \varphi\circ - x_C)^2 + ((0.06) \sin \varphi\circ - 0)^2 = 0.15^2$

with MATLAB command is: eqnC='(xB-xCsol)^2+(yB-yC)^2=BC^2';

where xCsol is the unknown. To solve the equation, a specific MATLAB command will be used. The command:

solve('eqn1','eqn2',...,'eqnN','var1','var2',...'varN')

 attempts to solve an equation or set of equations 'eqn1','eqn2',...,'eqnN' for the variables 'eqnN','var1','var2',...'varN'. The set of equations are symbolic expressions or strings specifying equations. The MATLAB command to find the solution xCsolofXcis :

solC=solve(eqnC,'xCsol');

Because it is a quadratic equation two solutions are found for the position of C. The two solutions are given in a vector form: solC is a vector with two components solC(1) and solC(2). To obtain the numerical solutions the eval command has to be used:

xC1=eval(solC(1));

xC2=eval(solC(2));

 The command eval(s), where s is a string, executes the string as an expression or statement. The two solutions for xC

To determine the correct position of the joint C for the mechanism, an additional condition is needed.

For the first quadrant, $0 \le \varphi \le 90\circ$, the condition is xC>xB. This MATLAB condition

14

for xC located in the first quadrant is:

if xC1 >xBxC = xC1; else xC = xC2; end

The angle of the link 2 (link BC) with the horizontal inThe MATLAB expression for the angle $\varphi 2$ is: phi2 = atan((yB-yC)/(xB-xC));

1.3. Path of a Point C with General Plane Motion

The link 2 (connecting rod BC) has a general plane motion: translation along the x-axis, translation along the y-axis, and rotation about the z-axis. The mass centre of link 2 is located at C2. I've determined the path of point C2 for a complete rotation of the driver link 1.

The coordinates of the joint B are

x_B = ABcosφ and y_B = ABsinφ,

where $0 \leq \varphi \leq 360°$. The coordinates of the joint C are

$x_C = x_B + \sqrt{(BC^2 - y_B^2)}$ and $y_C = 0$.

 The mass center of the link 2 is the midpoint of the segment BC $x_{C2} = (x_B + x_C)/2$ and $y_{C2} = (y_B + y_C)/2$. The MATLAB statements for the coordinates of C2 are:

AB = 0.06 ; BC = 0.15; xA = 0; yA = 0; yC = 0;

incr = 0;

for phi=0:pi/100:2*pi, xB = AB*cos(phi);

yB = AB*sin(phi);

xC = xB + sqrt(BC^2-yB^2);

incr = incr + 1; xC2(incr)=(xB+xC)/2;

yC2(incr)=(yB+yC)/2; end
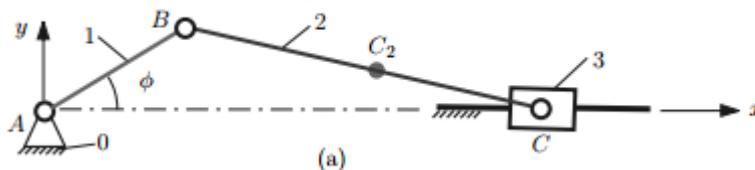
Figure 8:Mechanism points

For the complete rotation of the driver link AB, $0 \leq \varphi \leq 360°$, a step angle of $\pi/10$ was selected. For the coordinates of C2 two vectors:

xC2=[xC2(1) xC2(2) ... xC2(incr) ...]

yC2=[yC2(1) yC2(2) ... yC2(incr) ...]

are obtained. The first components xC2(1) and yC2(1) are calculated for phi=0 and incr=1.

The path ofC2 is obtained by plotting the vector yC2 in terms of xC2

15
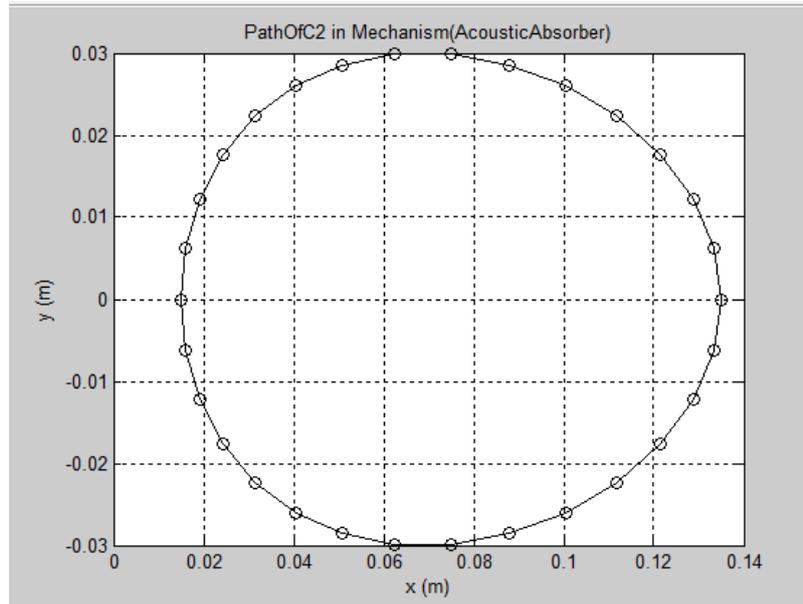
Figure 9:Path of C2

plot(xC2, yC2, '-ko'),...
xlabel('x (m)'), ylabel('y (m)'),...
title('Path described by C2'), grid

1.4. Velocity and acceleration analysis

The point A is selected as the origin of the xyz reference frame. The position vectors of the joints B and C are:

$r_B = x_B \mathbf{i} + y_B\ \mathbf{j} = \cos\varphi\mathbf{i} + \sin\varphi\mathbf{j}$ (m) and $r_C = x_C\mathbf{i} + y_C\mathbf{j} = \tan\varphi\mathbf{i} + 0\mathbf{j}$ (m) .
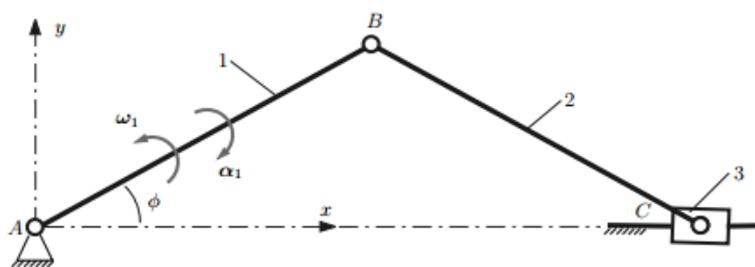
Figure 10:Velocity and Acceleration

Matlab code:

xA = 0; yA = 0; rA = [xA yA 0]; xB = AB*cos(phi); yB = AB*sin(phi);
rB = [xB yB 0]; yC = 0;
xC = xB+sqrt(BC^2-(yC-yB)^2);
rC = [xC yC 0];

16

1.5. Velocity of Joint B:

The velocity of the point B = B1 on the link 1 is

$v_B = v_{B1} = v_A + v_{BA} = v_A + \omega_1 \times r_{AB} = \omega_1 \times r_B$, where $v_A \equiv 0$ is the velocity of the origin A $\equiv$ O.

The velocity of point B_2 on the link 2 is $v_{B2} = v_{B1}$ because the links 1 and 2 are connected at a rotational joint. The velocity of B1 = B2 is

$$v_B = v_{B_1} = v_{B_2} = \begin{vmatrix} i & j & k \\ 0 & 0 & \omega_1 \\ x_B & y_B & 0 \end{vmatrix} \tag{1.1}$$
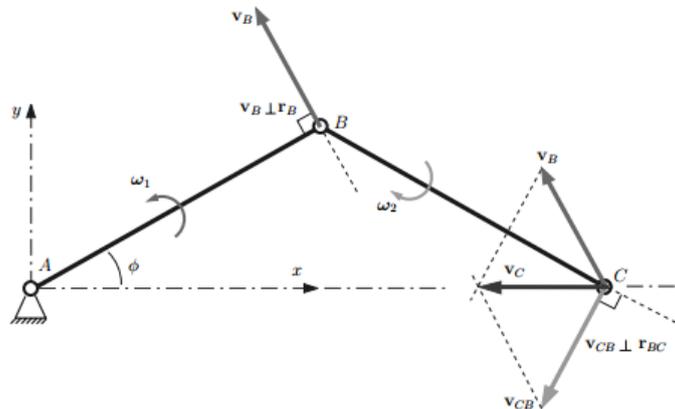
Figure 11:Velocity and acceleration directions

1.6. Velocity of Joint C:

The points B_2 and C_2 are on the link 2 and where the angular velocity of link 2 is $\omega_2 = \omega_2 k$ (ω_2 is unknown). On the other hand, the velocity of C is along the vertical axis (x-axis) because the slider 2 translates along the x-axis

$$v_B + \begin{vmatrix} i & j & k \\ 0 & 0 & \omega_2 \\ x_C - x_B & y_C - y_B & 0 \end{vmatrix} = v_C l. \tag{1.2}$$

$v_C = v_{C3} = v_C \mathbf{l}$

The above equations give: $v_B + \omega_2 \times (r_C - r_B) = v_C \mathbf{l}$Or

This equation represents a vectorial equation with two scalar components on x-axis and y-axis and with two unknowns ω_2 and v_C

$v_{Bx} - \omega_2 (y_C - y_B) = v_C,$

$v_{Bx} + \omega_2 (x_C - x_B) = 0,$

It's obtainable from two equations.

The relative velocity of point C with respect to B is :$v_{CB} = \omega_2 \times (r_C - r_B)$

In MATLAB the sym command constructs symbolic variables and expressions. The

commands: *omega2z = sym('omega2z','real');*
vCx = sym('vCx','real');

1.7. Dynamic analysis:

The equations of motion of a slider-crank mechanism may be formulated in various ways. Here, I formulate the equations of motion for the system shown below and impose the necessary constraints to form the slider-crank mechanism. The system as previously described, consists of two links and an end mass. The system is driven by a torque T on the shaft at A. It is assumed that the end mass m3 translates but does not rotate.
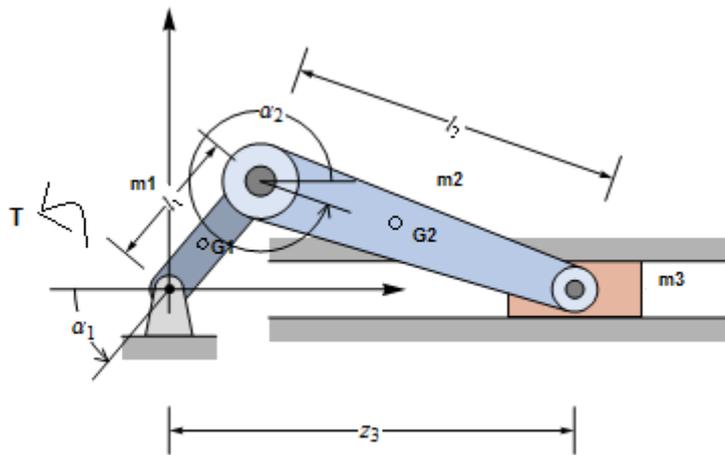
Figure 12:Dynamic analysis of mechanism

To convert the system shown into a simple slider-crank mechanism with zero offset, we require

. $l_1 \sin\alpha_1 + l_2 \sin\alpha_2 = 0$;

This constraint may be put into standard form by differentiating with respect to time to get

$(l_1\cos\alpha_1)\dot{\alpha}_1 + (l_2 s\cos\alpha_2)\dot{\alpha}_2 = 0$ (**)

1.8. Equations of Motion:

Using Lagrange's equations with multipliers, the equations of motion of the slider-crank mechanism may then be written in the form

$$\frac{d}{dt}\left(\frac{\partial L}{\partial \dot{\theta}_i}\right) - \frac{\partial L}{\partial \theta_i} = F_{\theta_i} + \lambda_1 a_{1i} \qquad (i=1,2) \qquad (1.3)$$

Where:

18

$(a_{11} = l_1\cos\alpha_1)$ and $(a_{12} = l_1\cos\alpha_1)$

Including the kinetic energies of the three bodies and the potential energies associated with the weight forces, it can be shown (α

$$\frac{d}{dt}\left(\frac{\partial L}{\partial \dot{\theta}_1}\right) - \frac{\partial L}{\partial \theta_1} = (m_1 r_1^2 + I_1 + m_2 l_1^2 + m_3 l_1^2)\ddot{\theta}_1 + (m_2 l_1 r_2 + m_3 l_1 l_2) - \cos(\theta_2 - \theta_1)\ddot{\theta}_2 \qquad (1.4)$$

$$+ (m_2 l_1 r_2 + m_3 l_1 l_2)\sin(\theta_2 - \theta_1)\dot{\theta}_2^2 + (m_1 r_1 + m_2 l_1 + m_3 l_1)g\cos(\theta_1)$$

$$\frac{d}{dt}\left(\frac{\partial L}{\partial \dot{\theta}_2}\right) - \frac{\partial L}{\partial \theta_2} = (m_2 l_1 r_2 + m_3 l_1 l_2)\cos(\theta_2 - \theta_1)\ddot{\theta}_1 + (m_2 r_2^2 + I_2 + m_3 l_2^2)\ddot{\theta}_2 \qquad (1.5)$$

$$+ (m_2 l_1 r_2 + m_3 l_1 l_2)\sin(\theta_2 - \theta_1)\dot{\theta}_1^2 + (m_2 r_2 + m_3 l_2)g\cos(\theta_2)$$

The contribution of the driving torque to the equations of motion are

$$F_{\theta_1} = T\underline{k}.\partial\,\underline{\omega}_1/\partial\dot{\theta}_1 = T \qquad (1.6)$$

$$F_{\theta 2} = T\underline{k}.\partial\,\underline{\omega}_1/\partial\dot{\theta}_2 = 0 \qquad (1.7)$$

Using these results in the equations of motion gives the final results

$$(m_1 r_1^2 + I_1 + m_2 l_1^2 + m_3 l_1^2)\ddot{\theta}_1 + (m_2 l_1 r_2 + m_3 l_1 l_2)\cos(\theta_2 - \theta_1)\ddot{\theta}_2 \qquad (1.8)$$

$$+ (m_2 l_1 r_2 + m_3 l_1 l_2)\sin(\theta_2 - \theta_1)\dot{\theta}_2^2 + (m_1 r_1 + m_2 l_1 + m_3 l_1)g\cos(\theta_1) = T + \lambda_1 l_1\cos(\theta_1)$$

$$(m_2 l_1 r_2 + m_3 l_1 l_2)\cos(\theta_2 - \theta_1)\ddot{\theta}_1 + (m_2 r_2^2 + I_2 + m_3 l_2^2)\ddot{\theta}_2 \qquad (1.9)$$

$$+ (m_2 l_1 r_2 + m_3 l_1 l_2)\sin(\theta_2 - \theta_1)\dot{\theta}_1^2 + (m_2 r_2 + m_3 l_2)g\cos(\theta_2) = \lambda_1 l_2\cos(\theta_2)$$

These two above equations must be solved simultaneously with the constraint equation, so we differentiate equation (**) again, giving the third differential equation

$$(l_1\cos(\theta_1))\ddot{\theta}_1 + (l_2\cos(\theta_2))\ddot{\theta}_2 - (l_1\sin(\theta_1))\dot{\theta}_1^2 - (l_2\sin(\theta_2))\dot{\theta}_2^2 = 0 \qquad (1.10)$$

form a set of three coupled, second-order, differential/algebraic equations that can be solved for the three unknowns $\theta 1$, $\theta 2$, and $\lambda 1$ as functions of time given the driving torque T and an initial position.

1.9. Membrane analysis:

First I would try to recall the Circular Membrane Problem by considering its characteristics and mechanical properties.

1.10. Normal modes of Circular Membrane:

The shape of an ideal vibrating thin elastic membrane stretched over a circular frame of radius a can be modelled by

$$u_{tt} = c^2 \nabla^2 u, \qquad x^2 + y^2 < a^2, \tag{1.11}$$

$$u(x, y, t) = 0, \quad x^2 + y^2 = a^2. \tag{1.12}$$

We can put it in polar coordinates this takes the form

$$u_{tt} = c^2 \left(u_{rr} + \frac{1}{r} u_r + \frac{1}{r^2} u_{\theta\theta} \right), \qquad 0 \le r < a, \, t > 0, \tag{1.13}$$

$$u(a, \theta, t) = 0, \qquad 0 \le \theta \le 2\pi, \tag{1.14}$$

$$u(r, 0, t) = u(r, 2\pi, t), \tag{1.15}$$

$$u_\theta(r, 0, t) = u_\theta(r, 2\pi, t), \qquad 0 \le r \le a, \, t \ge 0. \tag{1.16}$$

We will also impose the initial conditions

$$u(r, \theta, 0) = f(r, \theta), \qquad 0 \le r \le a, 0 \le \theta \le 2\pi, \tag{1.17}$$

$$u_t(r, \theta, 0) = g(r, \theta), \qquad 0 \le r \le a, 0 \le \theta \le 2\pi, \tag{1.18}$$

Which give the initial shape and initial velocity of the membrane, respectively. My eventual goal is to completely solve this problem in the usual manner:

First use separation of variables to find the simplest solutions to polar coordinates form equations

Then use superposition to build series solutions that satisfy initial condition as well.

Setting u(r, θ,t) = R(r)Θ(θ)T(t) leads to the separated boundary value problems

$$r^2 R'' + rR' + (\lambda^2 r^2 - \mu^2)R = 0, \qquad R(a) = 0, \tag{1.19}$$

$$\Theta'' + \mu^2 \Theta = 0, \qquad \begin{aligned} \Theta(0) &= \Theta(2\pi), \\ \Theta'(0) &= \Theta'(2\pi), \end{aligned} \tag{1.20}$$

$$T'' + c^2 \lambda^2 T = 0. \tag{1.21}$$

So the solution will be:

$$\Theta(\theta) = \Theta_m(\theta) = A_m \cos m\theta + B_m \sin m\theta, \quad \mu = m = 0, 1, 2, ..., \tag{1.22}$$

and that T(t) is a linear combination of $\cos c\lambda t$ and $\sin c\lambda t$.

To determine R and λ, it remains to solve the boundary value problem

$$r^2 R'' + rR' + (\lambda^2 r^2 - m^2)R = 0, \tag{1.23}$$

$$R(a) = 0. \tag{1.24}$$

The ODE above is the parametric form of Bessel's equation of order m. As we will see, it's general solution is given by

$$R(r) = c_1 J_m(\lambda r) + c_2 Y_m(\lambda r) \tag{1.25}$$

where J_m and Y_m are the Bessel functions of order m of the first and second kind, respectively.

By solving the Bessel function problem we find that the normal modes of the vibrating circular membrane can be written as:

$$u_{mn}(r, \theta, t) = J_m(\lambda_{mn} r)(a_{mn} \cos m\theta + b_{mn} \sin m\theta) \cos c \lambda_{mn} t, \tag{1.26}$$

$$u_{mn}^*(r, \theta, t) = J_m(\lambda_{mn} r)(a_{mn}^* \cos m\theta + b_{mn}^* \sin m\theta) \sin c \lambda_{mn} t \tag{1.27}$$

for m = 0, 1, 2, . . ., n = 1, 2, 3, . . ., where $\lambda_{mn} = \alpha_{mn}/a$ and α_{mn} is the nth positive zero of $J_m(x)$.

1.11. Role of Modelling and Simulation

Modelling and simulation of dynamic systems is a method for studying and developing a real system before it is being implemented in real life, it is a powerful tool for analysing the details of complex processes and the behaviour of the systems, its applications is not constrained by discipline boundaries and its complexity and results are dependent on the variety of available computing resources and the limits that a human thinking and the level of computational skills they can reach to. The role of system modelling can be used in various aspects, it assists the engineering design process and the decisions made about it, and it can also be a powerful educational and training tool for all levels that gives a better understanding of the real life physical systems. Physical models of acoustical-mechanical, thermo electrical, electro-mechanical or a combination of these systems can be constructed, designed and modified easily using simulation and modelling software. For example the accuracy of the computations of the mechanisms properties is a major importance for many

scientific and industrial applications, sound absorber which are mainly used for the purpose of noise reduction systems requires to have precise calculations of the acoustical properties of the environment, these calculations where previously done manually using a pencil and paper, but nowadays specialised computer software's such as MATLAB arise to replace the old methods and to provide a quick and accurate way of calculating these properties, moreover the SIMULATION models gives the advantage to simulate the physical models and process and its results before it is implemented in real life application.

1.12. Simulation of Crank slider Mechanism with Membrane Using MATLAB-SIMULINK

The model develops a simulation of a Crank slider mechanism wich is connected to a non-linear Spring that is very good estimation for the membrane analysis and also investigates analogues of the displacement and velocity of the model .It also investigates how different domains (Mechanical, acoustical) can be related to each other as analogues and how the energy is stored and released from one domain to the other.

The concept of a modelling is used to explain how energy can be stored and released from one domain to the other. An example is developed of a nonlinear spring attached to a crank slider mechanism model where energy is transformed from the strain energy domain to the kinetic energy domain and this is modelled in SIMULINK.

The kinematics and equations of the crank slider -Piston Cylinder mechanism were also studied and modelled. This example is to explain how energy is transformed between a mechanical and acoustical domain.

1.13. Non-Linear spring as a membrane

The first stage of the project is to analyse a crank slider mechanism attached to a non-linear spring, in this case the non-linear spring force behaves in a similar way as the membrane which is using to absorb the low frequencies noise.

For a nonlinear spring the relation between the force and displacement is given by the following equation:

$$F(x) = K.X + B.X^3 \tag{1.28}$$

Where

K: Linear Spring Constant (N/m)

B: Non linear Spring Constant (N/m) –can be positive (Hardening spring) or negative (Softening spring)

X: Displacement of the spring (m)

Figure 13 shows the diagram of a nonlinear spring compared to that of a linear spring;

the difference between both springs is with the non-linear term in the non-linear spring force equation, the linear spring will behave in a linear fashion and hence will have a unique slope whereas the non-linear spring will have different response at different displacements and hence different slopes depending on the value of the force the spring is subjected to and the spring type (Hardening/Softening).

$$K = K_o + K_n \tag{1.29}$$
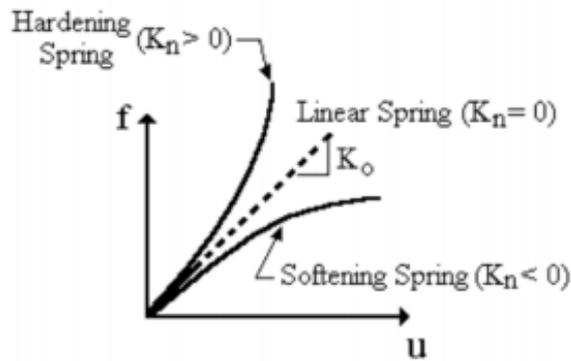
Figure 13:Force-Displacement Relationship for Single degree of freedom

1.14. Crank Slider-Nonlinear spring dynamic analysis

The schematic diagram of a typical crank slider mechanism is shown in Figure 14, the crank is driven by constant velocity source; the slider is moving against a nonlinear spring, the spring is initially unstrained (at $\theta=0^0$).
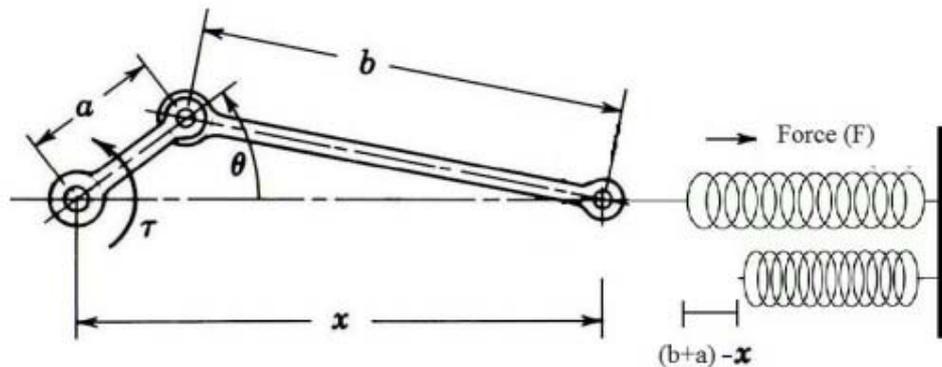
Figure 14: Modelling the membrane as a nonlinear spring

The following table are the constants used in the SIMULINK Block diagram of the crank slider mechanism attached to a nonlinear (hardening spring):

Table 1.1. Data inputs for the Crank slider-Nonlinear spring SIMULINK model

Input	Value
Initial Angular Velocity (ω0)	10 (rad/seconds)
Polar moment of inertia (J)	100 (m^4)
Crank Slider Length (a)	0.3 (m)
Connecting rod Length (b) *	1.2 (m)
Linear Spring constant (K)	100 (N/m)
Non-Linear Spring constant(B)	15
Number of cycles	$1=360^0$
initial conditions	Θ=0

*For Smooth Velocity response the length of the Connecting rod b is assumed to be 4 times the crank slider length a.

The deflection of the spring can be found from the geometry of the crank slider mechanism it can be written in the following form

$$\text{Spring Deflection} = (b+a) - X = a - a.\cos(\theta) + L - L.\cos(\varphi) \qquad (1.30)$$

From the geometry, it can be seen that

$$a.\sin(\theta) = b.\sin(\varphi) \qquad (1.31)$$

Using Pythagoras rule, it can be found that the spring deflection equation is obtained for any position of the angle θ as follows:

$$\text{Spring Deflection} = (b+a) - X = a - a.\cos(\theta) + b - \sqrt{b^2 - (a.\sin\theta)^2} \qquad (1.32)$$

Simulation of Crank slider mechanism with a Non-linear spring model

Figure 15:Crank slider mechanism attached to a nonlinear spring Block Diagram

Figure 16 shows the change of the crank slider displacement with respect to time, initially the displacement is at its maximum position (a + b=1.5 m) ,then it starts to decrease with the rotation of the crank slider until it reaches its minimum value of (0.9 m) which is the difference between the lengths of the connecting rod and twice the length of the crank slider(b-2.a), at that location the cranks slider have travelled half cycle (1800),the displacement then starts to increase again back to its initial value (1.5 m) and hence a complete full cycle (3600) is achieved, the cycle then repeats itself .

Figure 16:Crank slider mechanism Displacement (X) Vs Time

Figure 17 shows the change of the piston Linear velocity with respect to time, at the start of the simulation the linear velocity is zero , it then starts to increase until it reaches its maximum value of -3 m/second, at that location the cranks slider (a) have travelled 1/4th of a cycle (90 [0]) , the linear velocity then reduces back to zero where at that location the crank will have travelled half cycle (180^0) , after that the velocity starts to rise again up to 3 m/second and again returns back to zero at the end of the cycle and so on for the following cycles, the velocity sign change is to indicate that the velocity is acting in both direction of the X-axis.
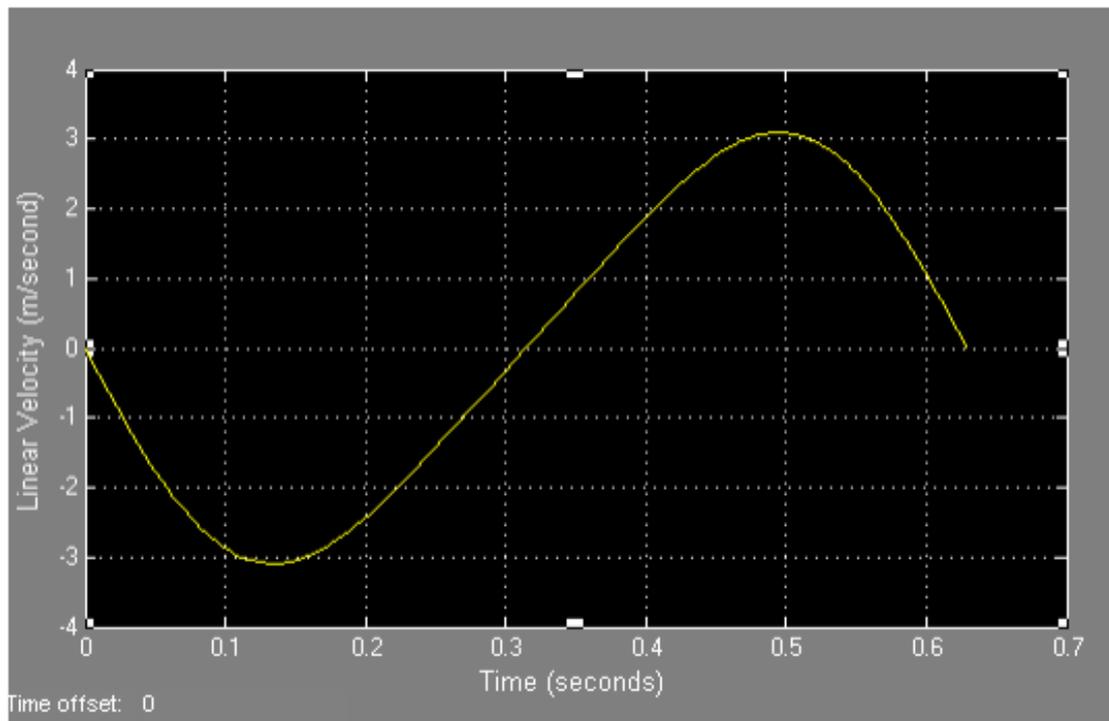
Figure 17:Linear Velocity Vs Time

Figure 18 shows the change of the crank angular velocity with respect to time, at the start of the simulation the angular velocity is at its initial value of 10 rad/second , it then slightly decrease until it reaches its minimum value 9.91 (rad/second) , at that location the cranks slider have travelled half a cycle (180^0) , then the angular velocity starts to increase again until it retains its initial value of 10 (rad/second) ,the reason behind the slight change in velocity is due to two reasons, the first reason is due to the nonlinear spring term in the spring equation which slightly effects the angular velocity result ,the second reason is related to the fact that the spring is always in tension which is opposing the angular velocity direction (the angular velocity direction is anti-clockwise whereas the spring force direction is clockwise, this difference causes a small reduction in the angular velocity .
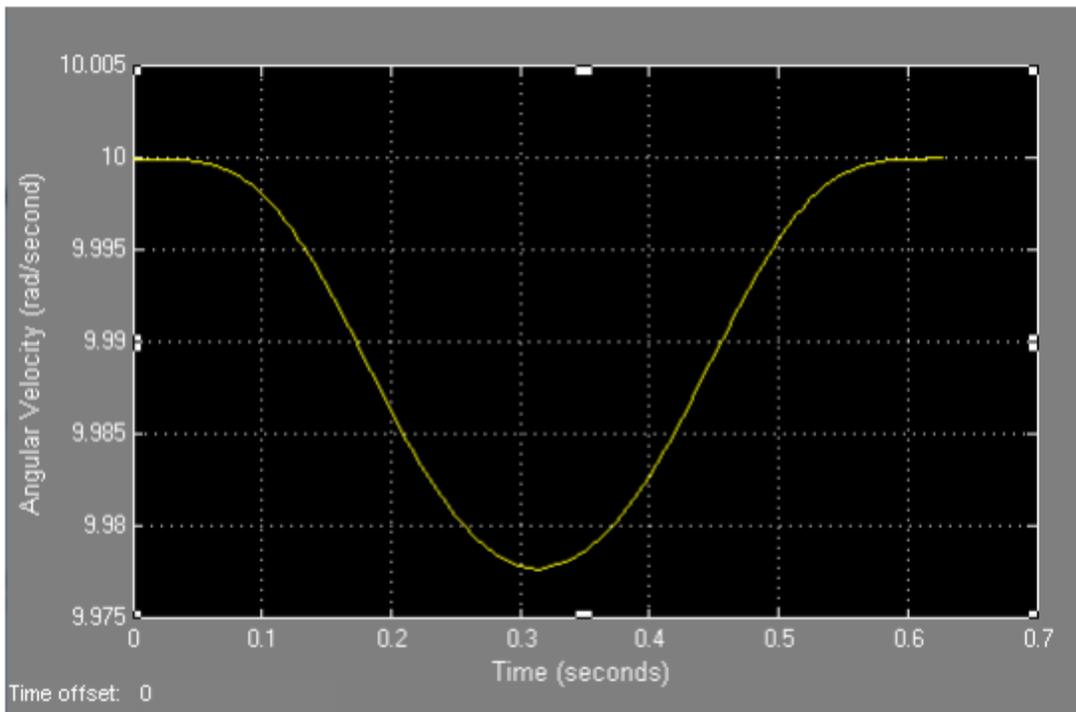
*Figure 18:Angular Velocity Vs Time*

Figure 19 shows the change of torque on crank arm with respect to time, at the start of the simulation there is no torque affecting the arm ,when the slider starts to move the torque starts increases until it reaches its maximum value of -13.9(N.m) , at that location the cranks slider have travelled 1/4th of a cycle (90 0) and then the torque returns back to zero where at that location the crank will have travelled half cycle (1800) ,the torque increase again to 13.9(N.m) and then goes back to zero at the end of the cycle and so on, it was noticed that the torque change in the 1st & 4th [0-π/2] &[2π/3-2π] quarters of the cycle is similar and differ from the similar 2nd and 3rd quarters of the cycle [π/2-π] &[π-2π/3] ,this is difference can be related to the fact that the polar moment of inertia is acting against the direction of motion along with the spring and hence there is some energy that is required to overcome the inertia of the system in order to enable the system to move ,this will result in a lower values of torques in those quarters compared to values of the torques in the other two quarters .
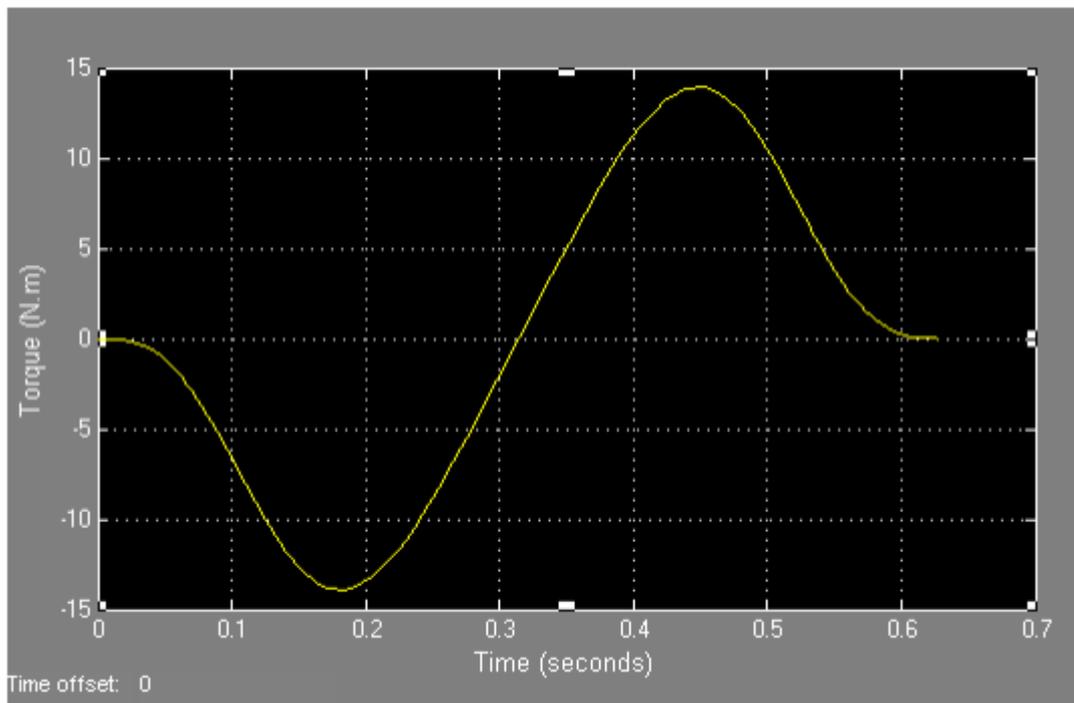
Figure 19: Torque Vs Time
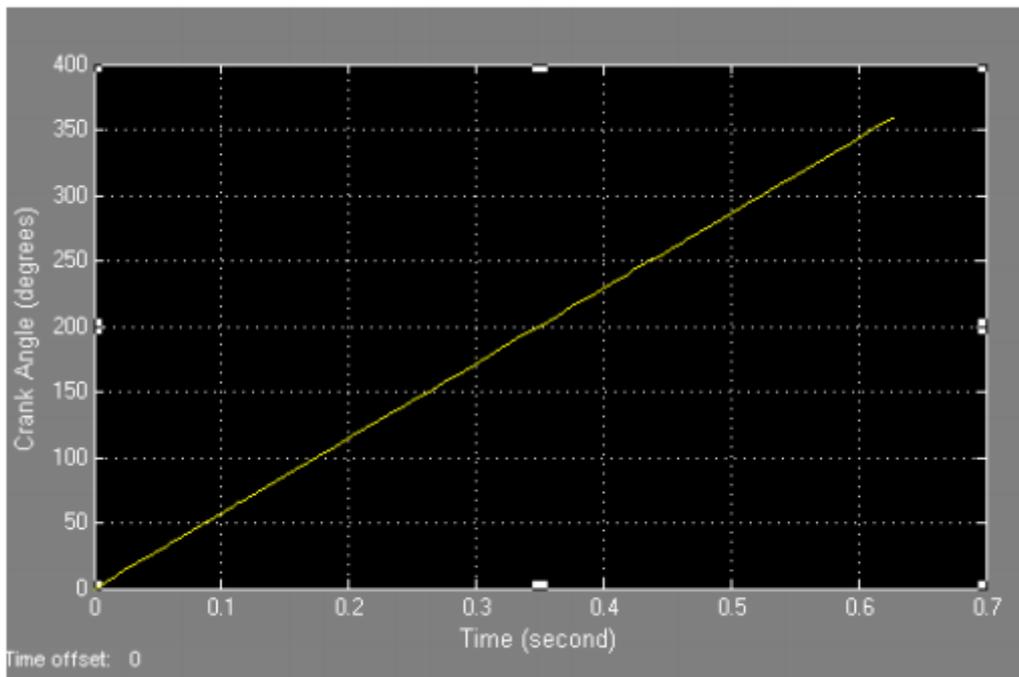
Figure 20: Crank Angle Vs Time

Figure 20 shows the change of the crank angle with respect to time for one revolution, the crank angel θ starts at 0 degrees and completes a full revolution of 3600 , the number of cycles is controlled by the (number of revolutions subsystem block, see Figure 21 ,it uses a stop command to stops the simulation at the desired number of revolutions, the number of revolutions can be increased or decreased by setting the number of revolutions in the [number of revolutions block] in the main SIMULINK model.
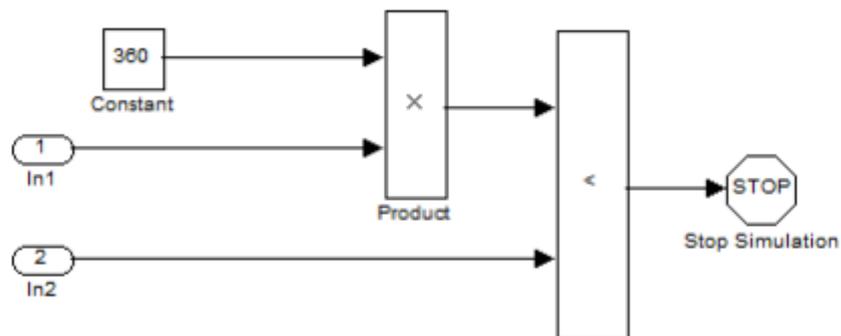
Figure 21:Number of revolutions control subsystem block diagram

30
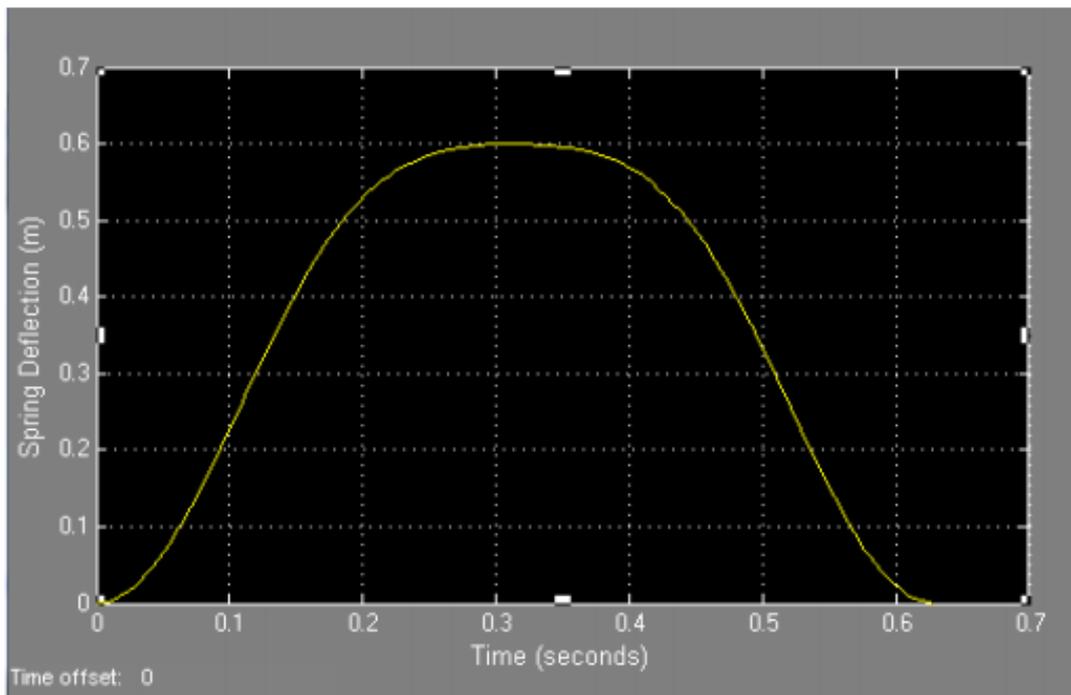
Figure 22:Spring deflection Vs Time

Figure 22 shows the spring deflection change with respect to time, at the start of the simulation the spring is un-strained, the spring starts to stretch with the change of the crank slider displacement for the a half revolution (0-π), in the second half of the cycle (π-2π) the spring length starts to decrease returning to its initial un-strained position.
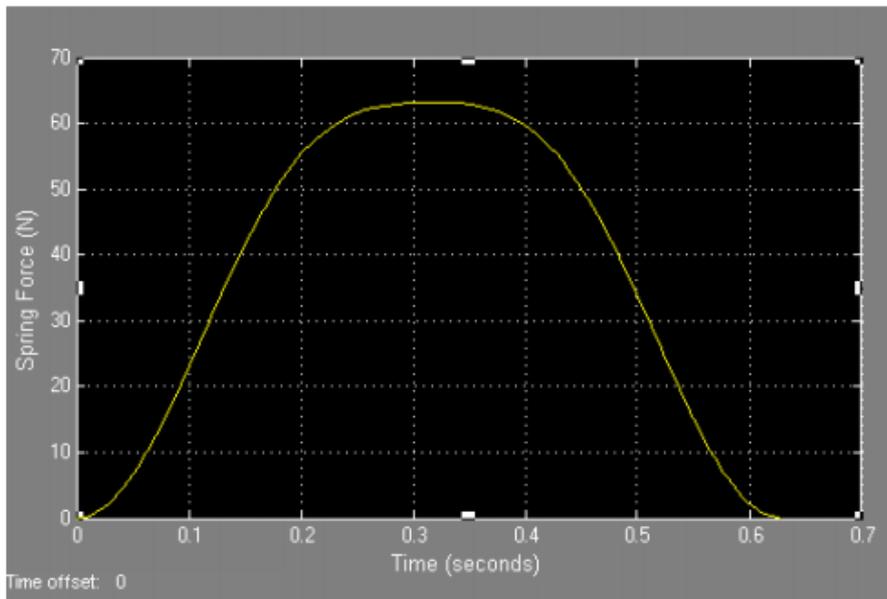
Figure 23:Spring Force Vs Time

Figure 23 shows the change in the spring force with respect to time, at the start of the simulation the spring is un-strained and there is no energy stored in the spring, it then starts to stretch with the change of the crank slider displacement for a half revolution (0-π) ,in the second half of the revolution (π-2π) the spring force starts to decrease returning it back to its initial un-strained position, the maximum force in the spring is 63.25 (N),this force is composed of the force due to the linear and non-linear terms in spring force equation, the force due to non-linear term is 3.25(N) and 60 (N) due to the linear term .
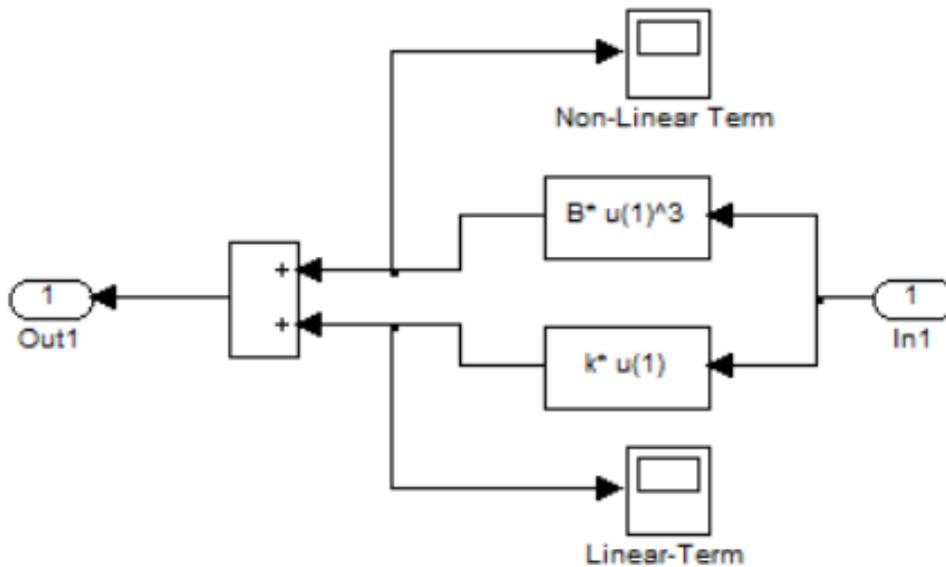
Figure 24:Non-Linear spring force subsystem

Figure 25 and Figure 26 shows the force in the spring due to these two terms individually.
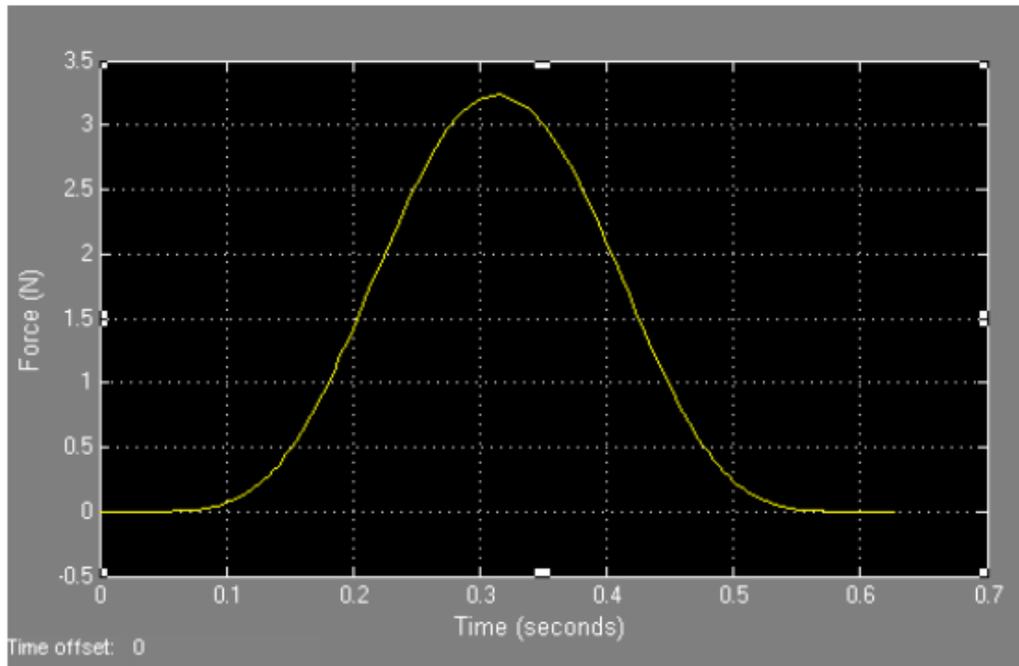
Figure 25: Nonlinear Spring force term Vs Time
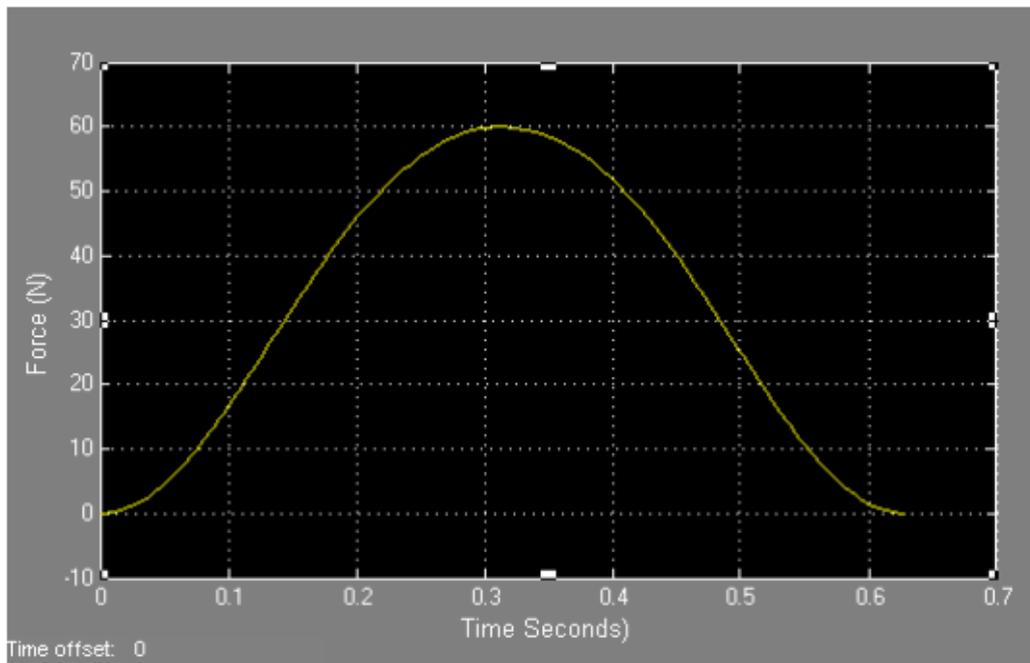
Figure 26: Linear Spring force term Vs time

33

Figure below 27 shows the plot of the spring force versus the spring displacement, it can be seen that the slope of the figure is nonlinear and that it becomes more non-linear with the increase of the displacement, it is also noticed that the nonlinear spring is a hardening spring where the force tends to increase faster with the increase of the displacement.
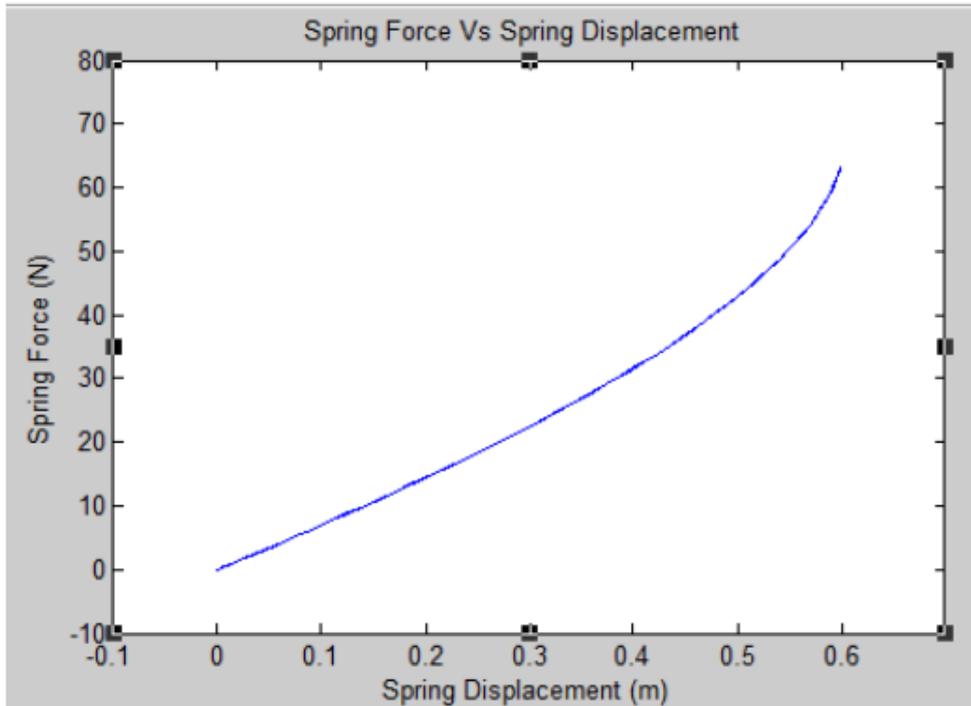
Figure 27:Spring Force Vs Spring displacement

Figure 28 shows the Linear Velocity/Angular Velocity (ARM) change with respect to time, the ARM value change from zero going to -0.31 (m/rad) at crank angle position (π/2) then it goes back to zero at (π) going up to 0.3 at (3π/2) going down to zero again at (2π),the figure shows that the change is the 1st and 4th quarters of the full revolution are different from the 2nd and 3rd quarters of the cycle , the reason behind that was explained in the discussion of the torque figure.
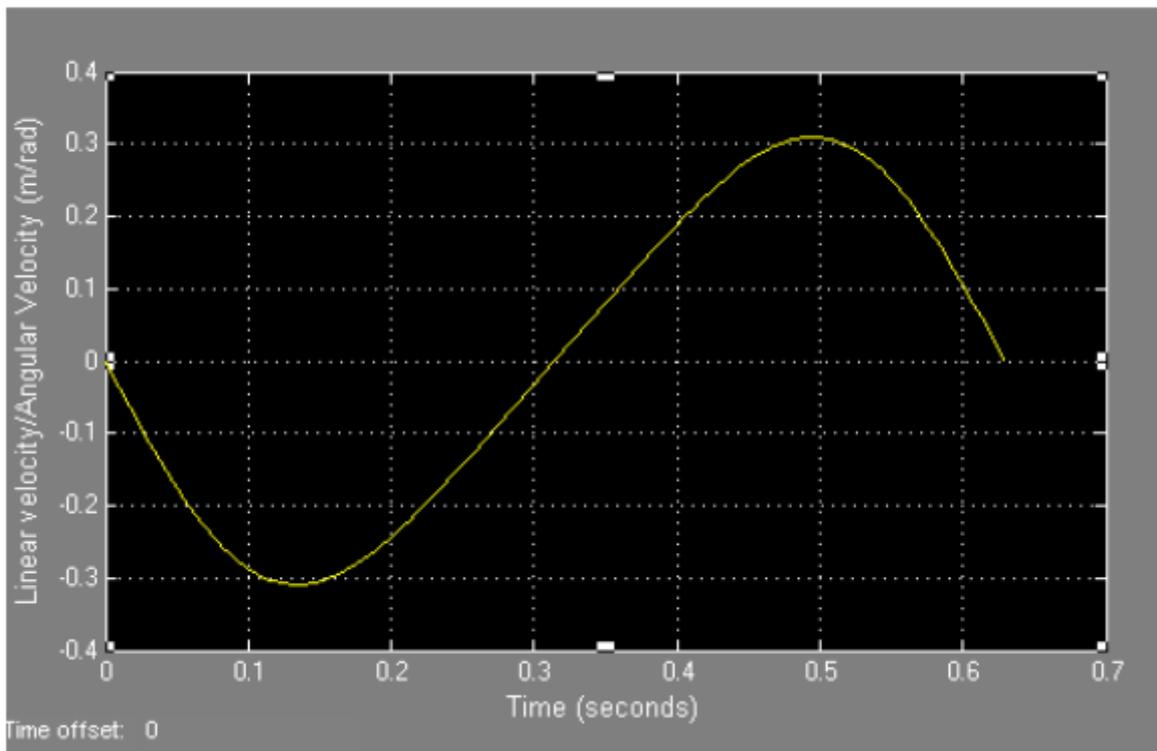
Figure 28:ARM (Linear Velocity/Angular Velocity) Vs Time

Acoustics:

2.1. Acoustics definition:

Acoustics is the science of sound, that is, wave motion in gases, liquids and solids, and the effects of such wave motion. Thus the scope of acoustics ranges from fundamental physical acoustics to, say, bioacoustics, psychoacoustics and music, and includes technical fields such as transducer technology, sound recording and reproduction, design of theatres and concert halls, and noise control.

2.2. Fundamental Acoustics Concepts:

One of the characteristics of fluids, that is, gases and liquids, is the lack of constraints to deformation. Fluids are unable to transmit shearing forces, and therefore they react against a change of shape only because of inertia. On the other hand a fluid reacts against a change in the volume with a change of the pressure. Sound waves are compressional oscillatory disturbances that propagate in a fluid. The waves involve molecules of the fluid moving back and forth in the direction of propagation (with no net flow), accompanied by changes in the pressure, density and temperature. The sound pressure, that is, the difference between the instantaneous value of the total pressure and the static pressure, is the quantity we hear. It is also much easier to measure the sound pressure than the other quantities. Note that sound waves are longitudinal waves, unlike bending waves on a beam or waves on a stretched string, which are transversal waves in which the particles move back and forth in a direction perpendicular to the direction of propagation. Sound waves exhibit a number of phenomena that are characteristics of waves; see figure 1. Waves propagating in different directions interfere; waves will be reflected by a rigid surface and more or less absorbed by a soft one; they will be scattered by small obstacles; because of diffraction there will only partly be shadow behind a screen; and if the medium is inhomogeneous for instance because of temperature gradients the waves will be refracted, which means that they change direction as they propagate. The speed with which sound waves propagate in fluids is independent of the frequency, but other waves of interest in acoustics, bending waves on plates and beams, for example, are dispersive, which means that the speed of such waves depends on the frequency content of the waveform.
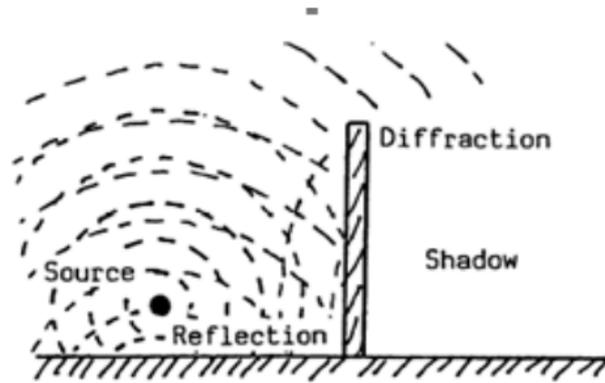
Joonis 2.1.Various wave phenomena

A mathematical description of the wave motion in a fluid can be obtained by combining equations that express the facts that i) mass is conserved, ii) the local longitudinal force caused by a difference in the local pressure is balanced by the inertia of the medium, and iii) sound is very nearly an adiabatic phenomenon, that is, there is no flow of heat. The result is the linearized wave equation. This is a second-order partial differential equation that, expressed in terms of the sound pressure p, takes the form

$$\frac{\partial^2 p}{\partial x^2} + \frac{\partial^2 p}{\partial y^2} + \frac{\partial^2 p}{\partial z^2} = \frac{1}{c^2}\frac{\partial^2 p}{\partial t^2} \qquad\qquad c = \sqrt{K_s/\rho}$$

(2.1)

In a Cartesian coordinate system the physical unit of the sound pressure is Pascal (1 Pa = 1 Nm-2). The quantity c, is the speed of sound. The quantity Ks is the adiabatic bulk modulus, and ρ is the equilibrium density of the medium.

2.3. Plane sound waves

The plane wave is a central concept in acoustics. Plane waves are waves in which any acoustic variable at a given time is a constant on any plane perpendicular to the direction of propagation. Such waves can propagate in a duct.

2.4. Acoustics Measurements

The most important measure of sound is the rms sound pressure defined as

$$p_{rms} = \sqrt{\overline{p^2(t)}} = \left(\lim_{T\to\infty} \frac{1}{T}\int_0^T p^2(t)dt \right)^{1/2}$$

(2.2)

However a frequency weighting filter is usually applied to the signal before the rms value is determined. Quite often such a single value does not give sufficient information about the nature of the sound, and therefore the rms sound pressure is determined in frequency bands. The resulting sound pressures are practically always compressed logarithmically and presented in decibels (dB).

2.5. Levels and decibels

The human auditory system can cope with sound pressure variations over a range of more than a million times. Because of this wide range, the sound pressure and other acoustic quantities are usually measured on a logarithmic scale. An additional reason is that the subjective impression of how loud noise sounds correlates much better with a logarithmic measure of the sound pressure than with the sound pressure itself. The unit is the decibel, abbreviated dB, which is a relative measure, requiring a reference quantity. The results are called levels. The sound pressure level (sometimes abbreviated SPL) is defined as

$$L_p = 10 \, \log_{10} \frac{p_{rms}^2}{p_{ref}^2} = 20 \, \log_{10} \frac{p_{rms}}{p_{ref}} \qquad (2.3)$$

Where pref is the reference sound pressure, and log10 is the logarithm to the base of 10, henceforth written log. The reference sound pressure is 20 µPa for sound waves in air. Some typical sound pressure levels are given in figure 2.2:
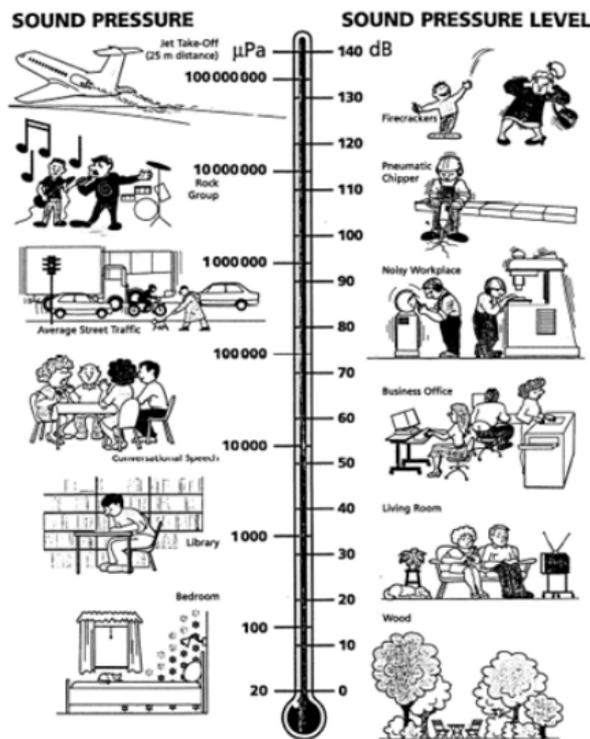
Joonis 2.2.Typical sound pressure level

2.6. Noise measurement techniques and instrumentation

A sound level meter is an instrument designed to measure sound pressure levels. Today such instruments can be anything from fairly simple devices with analogue filters and detectors and a moving coil meter to advanced digital analysers. Figure 4 shows a block diagram of a simple sound level meter. The microphone converts the sound pressure to an electrical signal, which is amplified and passes through various filters. After this the signal is squared and averaged with a detector, and the result is finally converted to decibels and shown on a display.
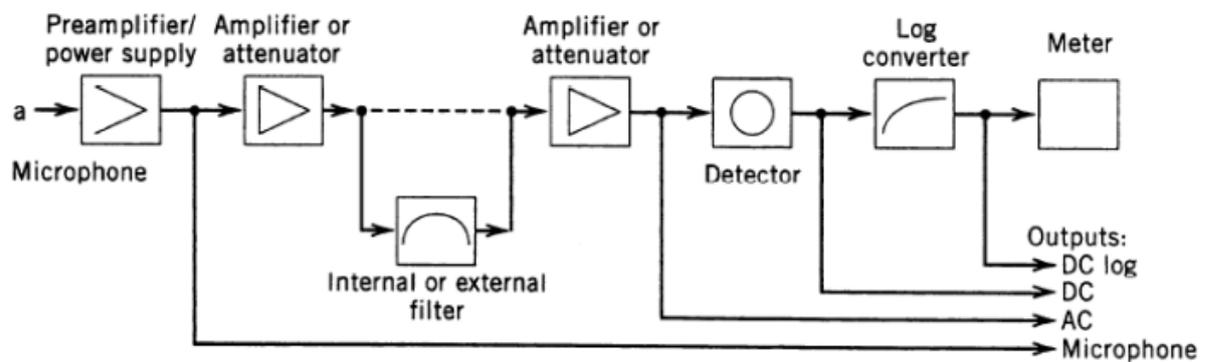
Joonis 2.3. Sound level meter

2.7. The Concept of Impedance

By definition an impedance is the ratio of the complex amplitudes of two signals representing cause and effect, for example the ratio of an AC voltage across a part of an electric circuit to the corresponding current, the ratio of a mechanical force to the resulting vibrational velocity, or the ratio of the sound pressure to the particle velocity. The acoustic impedance is associated with average properties on a surface. This quantity is mainly used under conditions where the sound pressure is more or less constant on the surface. It is defined as the complex ratio of the average sound pressure to the volume velocity, which is the surface integral of the normal component of the particle velocity. The acoustic impedance is:

$$Z_a = \hat{p}_{av}/\hat{q} \qquad (2.4)$$

The unit is $kgm^{-4}\ s^{-1}$

2.8. Duct Acoustics

2.8.1. Sound Radiation

Sound can be generated by many different mechanisms. The simplest one, which is also the most important: that of a solid vibrating surface. As I learned, the most efficient mechanism for radiation of sound involves a net volume displacement. The simplest source to describe mathematically is a sphere that expands and contracts harmonically with spherical symmetry.

2.8.2. Sound absorption

By definition the absorption coefficient of a given material is the absorbed fraction of the incident sound power. From this definition it follows that the absorption coefficient takes values between naught and unity. A value of unity implies that all the incident sound power is absorbed. In general the absorption coefficient of a given material depends on the structure of the sound field (plane wave incidence of a given angle of incidence, for example, or random or diffuse incidence in a room).

2.9. Absorption coefficient:

Sound Absorption Coefficient is the measure of how much sound is absorbed by a material. The absorption coefficient can be expressed as:

$(\alpha = 1 - I_R/I_i)$

(1) where α is the Sound Absorption Coefficient, I_R is the Reflected Sound Intensity and I_I is the Incident Sound Intensity.

Referring to above equation, it can be seen that the sound absorption coefficient, α, of materials are varies in the range of 0 to 1. Value 0 indicates zero sound absorption while value 1 indicates perfect sound absorption. In the case of $\alpha = 0$, the sound is completely deflected by the material.

On the other hand, $\alpha = 1$ represents that the sound is completely absorbed by the material.

2.10. Noise Reduction Coefficient.

Noise Reduction Coefficient, NRC is the arithmetic average value of the sound absorption coefficient at frequencies 250, 500, 1000 and 2000 Hz. It represents the ability of a material to absorb sound. Similar to α, NRC = 0 indicates a perfect sound deflection and NRC = 1 indicates a perfect sound absorption.

$$NRC = \frac{\alpha_{250} + \alpha_{500} + \alpha_{1000} + \alpha_{2000}}{4} \qquad (2.5)$$
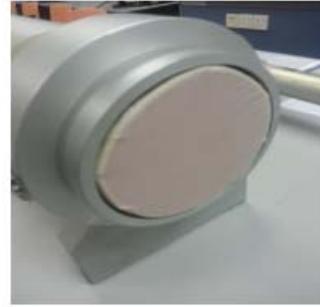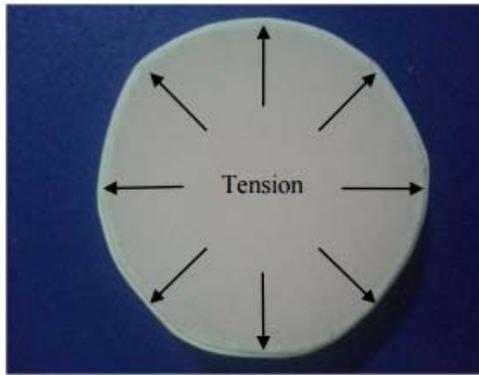
Joonis 2.4.

2.11. Experimental Analysis Specimens preparation

The specimens have been prepared in five surface tensions; 0 N, 50 N, 100 N, 150 N and 200 N respectively. Each of the surface tension has been prepared in 2 sizes; large and small. The large size specimen (100 mm in diameter) is for the low frequency test and the small size specimen (28 mm in diameter) is for the high frequency test. The thickness of the un-stretched membrane is 0.04 mm. Three specimens for all the membrane tensions were prepared for low and high frequency tests. The average values were then computed. An example of specimen used in the study was illustrated in Fig. 2.4 shows the specimen placement inside the impedance tube.

2.12. Effect on the Sound Absorption Coefficient,

α. Fig. 2.5(a)-(e) shows the effect of the membrane surface tension on the Sound Absorption Coefficient, α. Increasing the membrane surface tension make the sound absorption characteristics of the specimen less stable. These observations are due to the excessive vibration of the stretched membrane. The higher the membrane tension the more the vibration level is achieved. As depicted in Fig. 3 (a), the specimen with 0 N membrane surface tension performed the best in terms of stability and maximum α value which is 9.4 at 1600 Hz . However the curve is very steep hence the frequency range with good α value (≥0.8) is very narrow i.e. 1450 to 2000 Hz only. The membrane and the back-air cavity behave like a mass-spring-damper system. At 0 N condition, the sound pressure was in tuned with the mass-spring-damper system. As the tension was increased, the membrane-cavity become stiffer hence the sound pressure become less in tune with the mass-spring-damper system. At out of tuned conditions, the membranes vibrate chaotically which produced unstable absorption characteristics (Fig. 3 (b)-(d)).

42
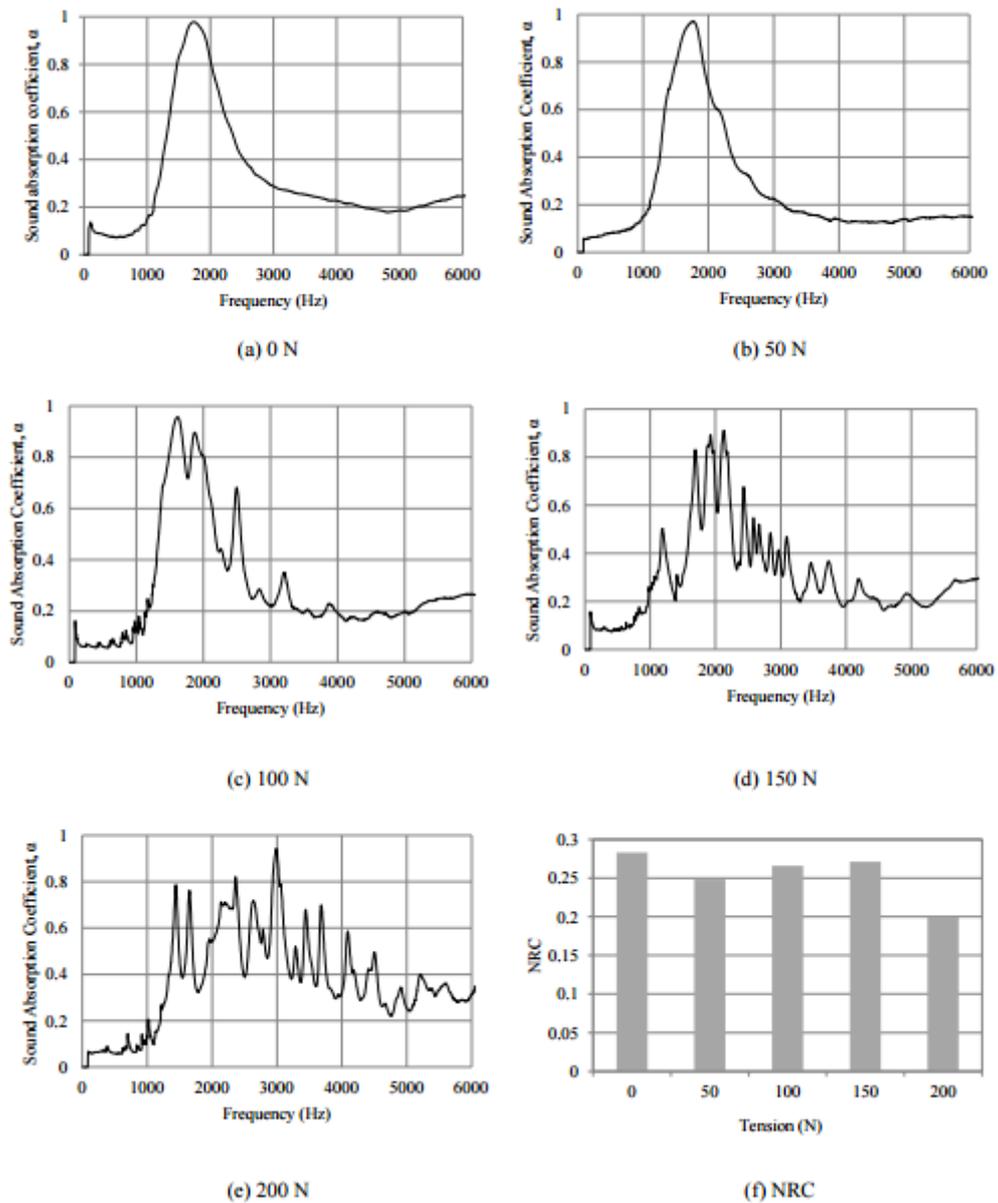
Joonis 2.5. Effect of membrane tension on the sound absorption characteristics.

2.13. Effect on the Noise Reduction Coefficient, NRC.

Fig. 2.5 shows the effect of membrane surface tension on the Noise Reduction Coefficient, NRC. The specimen with 0 N membrane surface tension has the best NRC value. The specimens with 100 N and 150 N surface tension seem to have good NRC values as well, however these values are not stable due to the fluctuations of its respective α values in Fig. 2.5 (c)-(d). The NRC values for all specimens never exceed 0.3 due to narrow frequency range of good α values. The maximum NRC value is 0.28 at 0 N surface tension.

The membrane surface tensions have significant influence on the sound absorption

characteristics. Membrane with non-stretched surface has better Sound Absorption Coefficient, α and Noise Reduction Coefficient, NRC values over the stretched membranes. The maximum α value obtained is very good which approximately 0.94 at 1600 Hz. The specimens' performance was at its best between 1450 to 2000 Hz. The NRC values for all specimens never exceed 0.3 due to the narrow frequency range of good α values. These findings indicate that for the parameter used in the laboratory work, the un-stretched membrane performed better in absorbing the sound energy.
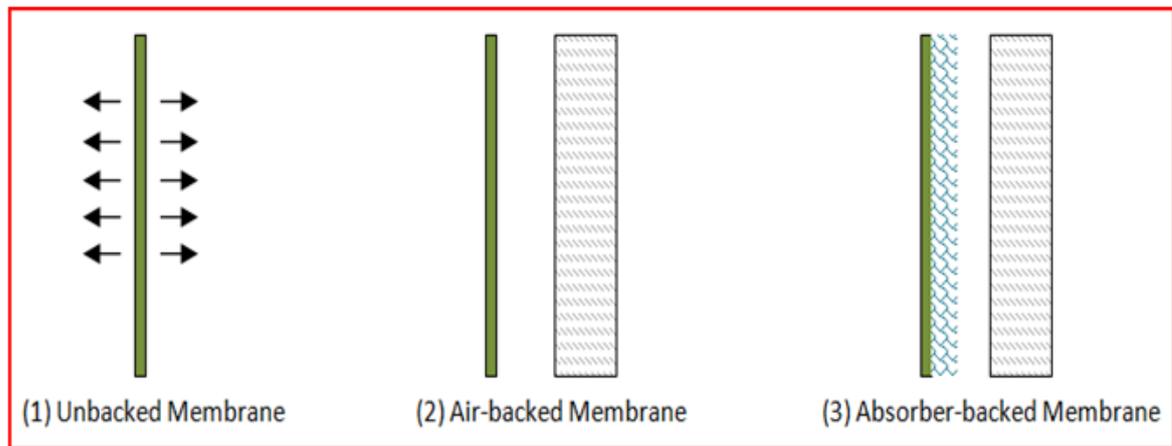
Joonis 2.6.

In the excel file there is a complicated effort to calculate the absorption coefficient in three types above, unbacked membrane, air-backed membrane and also absorber (porous material)-backed membrane.

CONTROL AND PROGRAMMING

3.1. Dynamic control analysis

The field-oriented PM synchronous motor drive The machine model of a PM synchronous motor can be described in the rotor rotating reference frame as follows [12]:

$$\upsilon_q = R_s i_q + p\lambda_q + \omega_s \lambda_d, \tag{3.1}$$

$$\upsilon_d = R_s i_d + p\lambda_d - \omega_s \lambda_q, \tag{3.2}$$

Where

$$\lambda_q = L_q i_q, \tag{3.3}$$

And

$$\lambda_d = L_d i_d + L_{md} I_{fd}. \tag{3.4}$$

In the above equations v d and v q are the d-, q-axis stator voltages, i d and i q are the d-, q-axis stator currents, ‚d and ‚q are the d-, q-axis inductances, j d and j q are the d-, q-axis stator flux linkages, while Rs and us are the stator resistance and inverter frequency respectively. The rotating reference d—q coordinates and the three-phase system are compared in Fig. 3. In Eq. (3.4) I fd is the equivalent d-axis magnetizing current, and ‚md is the d-axis mutual inductance. The electric torque

$$\tau_m = 3P\left[L_{md}I_{fd}i_q + (L_d - L_q)i_d i_q\right]/2, \tag{3.5}$$

and the equation for the motor dynamics is

$$\tau_e = \tau_m + B_m\omega_r + J_m p\omega_r. \tag{3.6}$$

In Eq. (5) P is the number of pole pairs, q m is the load torque, Bm is the damping coefficient, ur is the rotor speed and Jm is the moment of inertia. The inverter frequency is related to the rotor speed as

$$\omega_s = P\omega_r. \tag{3.7}$$
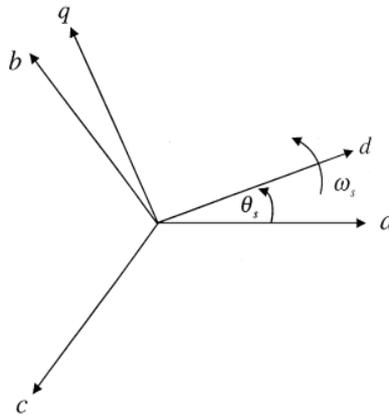
Joonis 3.1. Comparison of d—q coordinates with the three-phase system.

The basic principle in controlling a PM synchronous motor drive is based on field orientation. The flux position in the d—q coordinates can be determined by the shaft-position sensor because the magnetic flux generated from the rotor's permanent magnet is fixed in relation to the rotor shaft position. In Eqs. (3.4) and (3.5), if i d "0, the d-axis flux linkage j d is fixed since ¸md and I fd are constant for a PM synchronous motor, and the electromagnetic torque q e is then proportional to i q which is determined by closed-loop control. The rotor flux is produced in the d-axis only, while the current vector is generated in the q-axis for the field-oriented control. Since the generated motor torque is linearly proportional to the q-axis current as the d-axis rotor flux is constant in Eq. (3.5), the maximum torque per ampere can be achieved. The configuration of a general field-oriented PM synchronous motor drive system is shown in Fig. 4, which consists of a PM synchronous motor coupled with a mechanism, a ramp comparison current-controlled PWM voltage source inverter (VSI), a unit vector (cos h s = j sin h s , where h s is the position of rotor flux) generator, a coordinate translator, a speed control loop and a position control loop. The PM synchronous motor used in this drive system is a three-phase four-pole 750W 3.47 A 3000 rpm type. With the implementation of field-oriented control, the PM synchronous motor drive system can be simplified to a control system block diagram, as shown in Fig. 5, in which

$$\tau_e = K_t i_q^*, \tag{3.8}$$

$$K_t = \frac{3}{2} P L_{md} I_{fd}, \tag{3.9}$$

$$H_p(s) = \frac{1}{J_m S + B_m}. \tag{3.10}$$
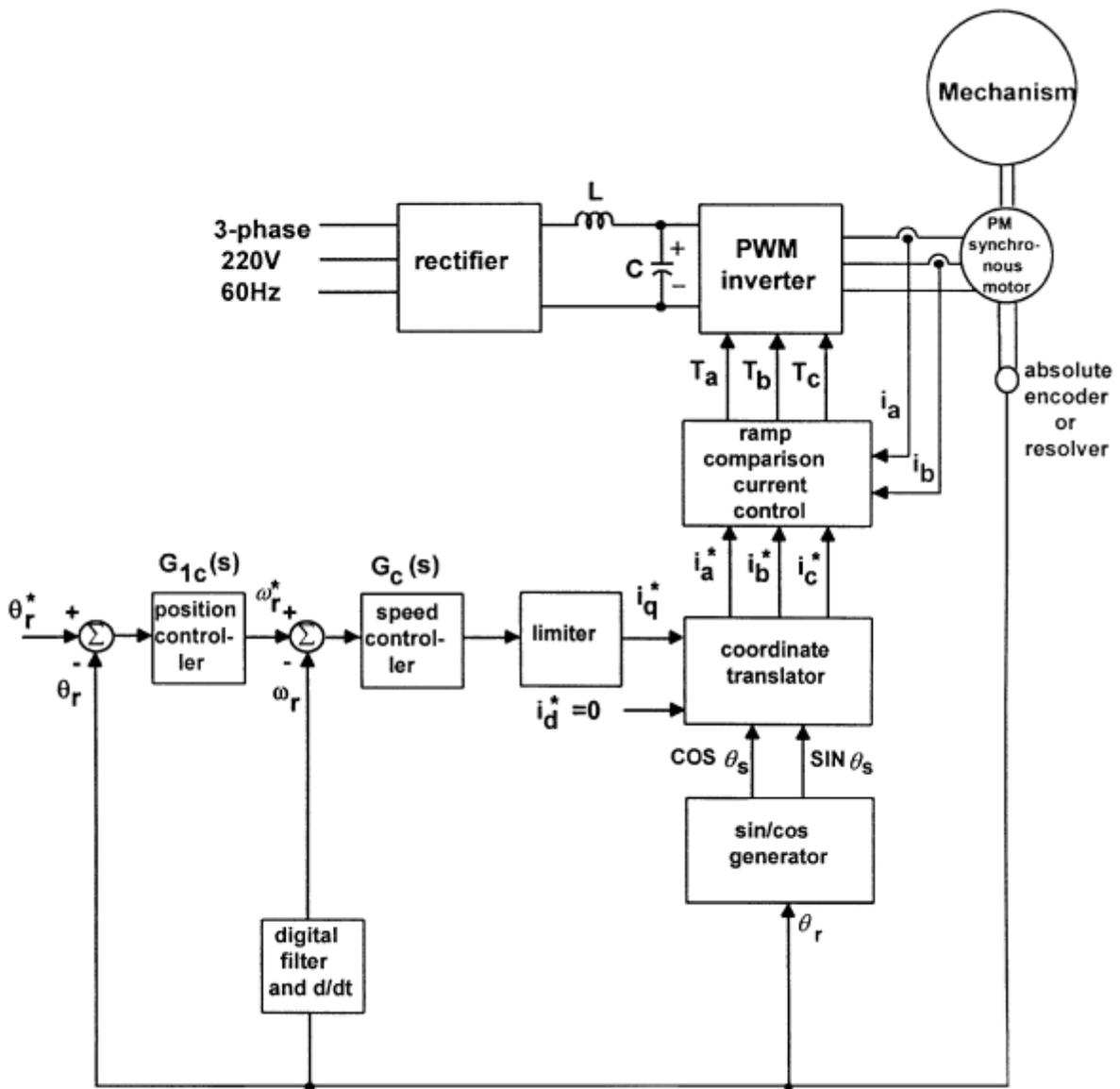
Joonis 3.2. Configuration of a field-oriented PM synchronous servo motor drive system.
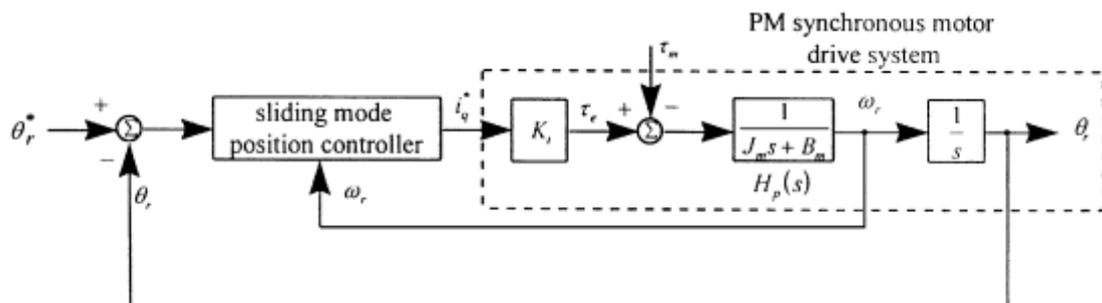
Joonis 3.3. Block diagram of a PM synchronous servo motor using the field-oriented mechanism with sliding mode controller

whereKt and i* q are the torque constant and torque current command, respectively. The sliding mode position controller, also shown in Fig. 5, will be discussed in the following section. For the convenience of the controller design, the position and speed signals in the control loop are set at 1 V"50 rad and 1 V"50 rad s$^{\sim 1}$·Fig. 1 shows a PM synchronous motor system including a geared speed-reducer with a gear ratio

$$n = \frac{n_a}{n_b} = \frac{\tau}{\tau_m} = \frac{\omega_r}{\omega} = \frac{\dot{\theta}_r}{\dot{\theta}}. \tag{3.11}$$

where n, n a and n b are the gear ratio and gear numbers. Substituting Eqs. (3.8) and (3.11) into Eq. (6), the following applied torque can be obtained:

$$\tau = n(\tau_e - J_m\dot{\omega}_r - B_m\omega_r) = n(K_t i_q^* - nJ_m\ddot{\theta} - nB_m\dot{\theta}), \tag{3.12}$$

where q is the torque applying in the angle h. The parameters of the motor system are:

$$K_i = 0.6732 \text{ Nm A}^{-1}, \ n = 1, \tag{3.13}$$

$$\bar{J}_m = 1.32{\times}10^{-3} \text{ Nm s}^2 = 0.066 \text{ Nms rad V}^{-1}, \tag{3.14}$$

$$\bar{B}_m = 5.78{\times}10^{-3} \text{ Nm s rad}^{-1} = 0.289 \text{ Nm V}^{-1}. \tag{3.15}$$

3.2. Mathematical model of the coupled mechanism in state space demonstration

The slider-crank mechanism driven by a PM synchronous servo motor is shown in Fig. 2. The Hamilton's principle and the Lagrange multiplier are used to derive the differential-algebraic equation for the slider—crank mechanism in Appendix A. The constraint position, velocity and acceleration equations (3.14)—(3.16) must hold. By using Eqs. (3.13)—(3.15) and (3.16), the following equation in the matrix form is obtained:

$$\begin{bmatrix} M & \Phi_\psi^T \\ \Phi_\Psi & 0 \end{bmatrix} \begin{bmatrix} \ddot{\psi} \\ \lambda \end{bmatrix} = \begin{bmatrix} BU + D(\psi) - N(\psi, \dot{\psi}) \\ \gamma \end{bmatrix}. \tag{3.16}$$

This is a system of differential-algebraic equations and the matrices element can be found in Appendix A.

3.3. Reduced system of differential equations of motion

The differential algebraic equation of mechanism motion derived above are summarized in the matrix form of Eq. (3.14), and the constraint equation of Eq. (A.4). Implicit method has to be employed to solve the equation of the system. Eqs. (3.14) and (A.4)

may be reordered and partitioned, according to the decomposition of t"[h /]T"[vTuT]T which is the same as . If the constraints are independent, the matrix Ut has full row rank, and there is always at least one non-singular submatrix Ut of rank 2. Gauss—Jordan reduction of the matrix Ut with double pivoting defines a partitioning of t"[vT, uT]T, u"[/]T, v"[h] such that Uu is the submatrix of Ut whose columns correspond to elements u of t and Uv is the submatrix of Ut whose columns correspond to element v of t. The elements of the vectors u, v and matrices Uu, Uv are detailed in the Appendix B. Thus, Eqs. (14) and(A4) can be rewritten as

$$M^{\upsilon u}\ddot{u} + M^{\upsilon\upsilon}\ddot{v} + \Phi_\upsilon^T\lambda = B^\upsilon U + D^\upsilon - N^\upsilon, \tag{3.17}$$

$$M^{uu}\ddot{u} + M^{u\upsilon}\ddot{v} + \Phi_u^T\lambda = B^u U + D^u - N^u, \tag{3.18}$$

$$\Phi_u\ddot{u} + \Phi_\upsilon\ddot{v} = \gamma, \tag{3.19}$$

Or in the matrix form as

$$\hat{M}(v)\ddot{v} + \hat{N}(v,\dot{v}) = \hat{Q}U + \hat{D}, \tag{3.20}$$

Where

$$\hat{M} = M^{\upsilon\upsilon} - M^{\upsilon u}\Phi_u^{-1}\Phi_\upsilon - \Phi_\upsilon^T(\Phi_u^{-1})^T[M^{u\upsilon} - M^{uu}\Phi_u^{-1}\Phi_\upsilon], \tag{3.21}$$

$$\hat{N} = [N^\upsilon - \Phi_\upsilon^T(\Phi_u^{-1})^T N^u] + [M^{\upsilon u}\Phi_u^{-1} - \Phi_\upsilon^T(\Phi_u^{-1})M^{uu}\Phi_u^{-1}]\gamma, \tag{3.22}$$

$$\hat{Q} = B^\upsilon - \Phi_\upsilon^T(\Phi_u^{-1})^T B^u, \quad U = [i_q^*], \quad \hat{D} = D^\upsilon - \Phi_\upsilon^T(\Phi_u^{-1})^T D^u. \tag{3.23}$$

The result is a set of differential equations with only one independent generalized coordinate l. The equation is a initial value problem and can be integrated by using the fourth order Runge—Kutta method.

3.4. State variable representation

Let X"[v, vR]Tbe the state variable vector, one can rewrite Eq. (16) as the state space dynamics as

$$\dot{X} = f(X) + GU(t) + d(t), \tag{3.24}$$

Where

$$f(X) = \begin{bmatrix} \dot{v} \\ -\hat{M}^{-1}\hat{N} \end{bmatrix}, \quad G = \begin{bmatrix} 0 \\ \hat{M}^{-1}\hat{Q} \end{bmatrix}, \quad d(t) = \begin{bmatrix} 0 \\ \hat{M}^{-1}\hat{D} \end{bmatrix}, \quad U(t) = \begin{bmatrix} i_q^* \end{bmatrix}. \tag{3.25}$$

3.5. Design of the sliding mode controller with fuzzy logic

Consider the second-order nonlinear, single-input—single-output (SISO) motor-mechanism coupled system:

$$\ddot{\upsilon}(t) = f(X;t) + G(X;t)U(t) + d(t), \tag{3.26}$$

Where

$$f(X;t) = -\hat{M}^{-1}\hat{N}, \quad G(X;t) = \hat{M}^{-1}\hat{Q}, \quad d(t) = \hat{M}^{-1}\hat{D}, \tag{3.27}$$

and U(t) is the control input i* q . It is assumed that the function f is not exactly known, but the extent of the imprecision *f is bounded by a known continuous function F(X; t). Similarly, the control gain G(X; t) is not exactly known, but is of constant sign and known bounds, i.e.

$$0 < G_{min} \leq G(X;t) \leq G_{max}. \tag{3.28}$$

In addition, disturbance d(t) is unknown, but is bounded by a known continuous function D(X; t). According to the above description, then

$$|f - \hat{f}| \leq F(X;t), \tag{3.29}$$

$$\frac{1}{\alpha} \leq \frac{\hat{G}(X;t)}{G(X;t)} \leq \alpha, \tag{3.30}$$

$$|d| \leq D(X;t), \tag{3.31}$$

Where f and G are nominal values of f and G, respectively, and

$$\alpha = \left(G_{max}\big/G_{min}\right)^{1/2}. \tag{3.32}$$

The control problem is to find a control law so that the state X can track the desired trajectories Xd in the presence of the uncertainties. Let the tracking error vector be

$$e = X - X_d = [e, \dot{e}]^T, \tag{3.33}$$

where Xd "[v d , vR d]^T, and the second derivative of v d is assumed to be zero. Let us define a sliding surface S(t) in the state space R2 by the scalar function s(X; t)"0, where

$$s(X,t) = Ce + \dot{e}, \quad C > 0. \tag{3.34}$$

The initial condition is

$$e(0) = 0. \tag{3.35}$$

The tracking problem mentioned above is to find a control law º(t) so that the state X remaining on the surface s(X, t)"0 for all t*0. 3.1.

3.6. Sliding mode control law design

In the design of the sliding mode control system, first is to find the equivalent control law, ºeq, which will keep the state of the system on the sliding surface. The equivalent control law is found by the following equation:

51

$$\dot{s}\,|_{U=U_{eq}} = 0. \qquad (3.36)$$

Assuming all uncertainties are zero, then

$$\hat{f} + \hat{G}U_{eq} + C\dot{e} = 0. \qquad (3.37)$$

Solving Eq. (25), one can obtain

$$U_{eq} = (\hat{G})^{-1}\hat{U}, \qquad (3.38)$$

where

$$\hat{U} = -\hat{f} - C\dot{e}. \qquad (3.39)$$

Thus, given sR, the dynamics of the system on the sliding surface for t*0 is given by

$$\ddot{\upsilon}(t) = -C\dot{e}. \qquad (3.40)$$

3.7. Hitting control law

design A Lyapunov function candidate is chosen as follows:

$$V = \frac{1}{2}s^2(X;t). \qquad (3.41)$$

It is shown below that, if there exists a positive constant such that

$$\dot{V} = \frac{1}{2}\frac{d}{dt}(s^2(X:t)) \leq -\eta\,|s|, \qquad (3.42)$$

then the state trajectories will hit the sliding surface s. In order to satisfy the hitting condition of Eq. (30) in the presence of uncertainties, the control law is chosen as follows:

$$U = U_{eq} + U_n, \qquad (3.43)$$

where

$$U_n = -(\hat{G})^{-1}K\,\text{sgn}(s), \qquad (3.44)$$

and

$$\text{sgn}(s) = \begin{cases} 1 & \text{if} \quad s > 0, \\ -1 & \text{if} \quad s < 0. \end{cases} \qquad (3.45)$$

Then, Eq. (30) becomes

$$s\dot{s} = s(f + GU + d + C\dot{e}) \leq -\eta\,|s|. \qquad (3.46)$$

Or equivalently,

$$[f + d + C\dot{e}]\text{sgn}(s) + GU\,\text{sgn}(s) \leq -\eta. \qquad (3.47)$$

Substituting Eqs. (3.44), (3.45), (3.46) and (3.43) into (3.47), the following equation is obtained:

$$[f - \hat{f} + d]\,\text{sgn}\,(s) + \left(\frac{G}{\hat{G}} - 1\right)\hat{U}\,\text{sgn}\,(s) - \frac{G}{\hat{G}}K \le -\eta. \qquad (3.48)$$

The optimal value of K that satisfies Eq. (3.48) is

$$K \ge \alpha(F + D + \eta) + (\alpha - 1)\,|\,\hat{U}\,|. \qquad (3.49)$$

To alleviate the chattering phenomenon, the quasi-linear mode controller which replaces the discontinuous control laws of Eq. (3.49) by a continuous control one inside a boundary layeraround the switching surface, is adopted. That is $U_n$in Eq. (3.49) is replaced by

$$U_n = -(\hat{G})^{-1}K\,\text{sat}\left(\frac{s}{\varepsilon}\right), \qquad (3.50)$$

where e'0 is the width of boundary, and the function of sat (s/e) is defined as

$$\text{sat}\left(\frac{s}{\varepsilon}\right) = \begin{cases} 1 & \text{if} \quad s > \varepsilon, \\ \dfrac{s}{\varepsilon} & \text{if} \quad -\varepsilon \le s \le \varepsilon, \\ -1 & \text{if} \quad s < -\varepsilon. \end{cases} \qquad (3.51)$$

This leads to tracking within a guaranteed precision e while allowing the alleviation of the chattering phenomenon.

3.8. Design of fuzzy

In the general sliding mode control, the upper bound of uncertainties, which include parametric variation and external load disturbance, must be available. However, the bound of the uncertainties is difficult to obtain in advance for practical applications. Therefore, a fuzzy sliding mode controller is proposed here, in which a PI-type [11] fuzzy inference mechanism is used to estimate the upper bound of uncertainties. The fuzzy inference mechanism can construct the estimation model of uncertainties. Comparing with a conventional estimator, the fuzzy inference mechanism uses prior expert knowledge to accomplish control object more efficiently. Replace K by Kf in Eq. (37), the following control law can be obtained:

$$U(t) = U_{eq} - (\hat{G})^{-1}K_f\,\text{sat}\left(\frac{s}{\varepsilon}\right), \qquad (3.52)$$

Where Kf is estimated by the fuzzy inference mechanism. Because the data manipulated in the fuzzy inference mechanism is based on fuzzy set theory, the associated fuzzy sets involved in the fuzzy control rules are defined as follows:

N: Negative   Z: Zero   P: Positive

NH: Negative Huge   NB: Negative Big   NM: Negative Medium

NS: Negative Small   ZE: Zero   PS: Positive Small

PM: Positive Medium   PB: Positive Big   PH: Positive Huge

and their universe of discourses are all assigned to be [-6, 6]. There is no universal method to determine their values. Therefore, trial and error is needed in practice. The significance of the universe of discourse is that the input variables belonging to respective universe of discourse are mapped from measured values with corresponding scaling factors. Moreover, the fuzzy inference mechanism will be simplified to build a decision look-up table by the mapping process. The membership functions for the fuzzy sets corresponding to switching surface s, sR and the change of the upper bound of uncertainties K_f are defined in Fig. 3.4.
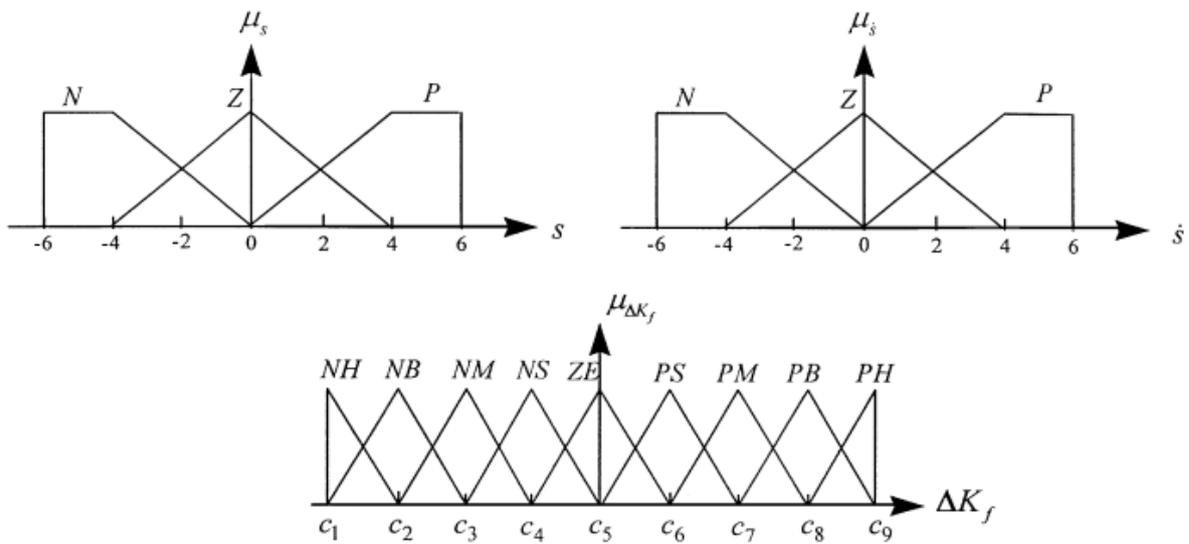

Joonis 3.4. Membership functions of s, $\dot{s}$ and ΔK_f

Since only three fuzzy subsets, N, Z and P, are defined for s and sR, the fuzzy inference mechanism only contains nine rules. The resulting fuzzy inference rules are as follows:

Rule 1: Is s is P and $\dot{s}$ is P Then ΔK_f is NH

Rule 2: Is s is P and $\dot{s}$ is Z Then ΔK_f is NB

Rule 3: Is s is P and $\dot{s}$ is N Then ΔK_f is NM

Rule 4: Is s is P and $\dot{s}$ is P Then ΔK_f is NS

Rule 5: Is s is P and $\dot{s}$ is Z Then ΔK_f is ZE

Rule 6: Is s is Z and $\dot{s}$ is N Then ΔK_f is PS

Rule 7: Is s is N and $\dot{s}$ is P Then ΔK_f is PM

Rule 8: Is s is N and $\dot{s}$ is Z Then ΔK_f is PM

Rule 9: Is s is N and $\dot{s}$ is N Then ΔK_f is PH

Rule 1 is the condition that the switching variable s is far away from the switching surface and the derivative of s is also positive, so a large *Kf is required for the occurrence of the sliding mode condition. Moreover, Rule 5 implies that the switching variable s is on the switching surface and the derivative of s is also zero, so only very small *Kf is required for the occurrence of the sliding mode condition. The same analysis can be used to explain the other fuzzy rules. Fuzzy output *Kf can be calculated by the center of area (COA) defuzzification as:

$$\Delta K_f = \frac{\Sigma_{i=1}^9 w_i c_i}{\Sigma_{i=1}^9 w_i} = [c_1 ... c_9] \begin{bmatrix} w_1 \\ \vdots \\ w_9 \end{bmatrix} \Big/ \sum_{i=1}^9 w_i = \upsilon^T W, \tag{3.53}$$

where t"[c 1 ,2, c 9] is the adjustable parameter vector; c 1 through c 9 are the center of the membership functions of K_f a firing strength vector. Then the upper bound of uncertainties can be obtained as follows:

$$K_f(k) = K_f(k-1) + \Delta K_f, \tag{3.54}$$

where k is the number of iterations.

Appendix

Appendix A

In this appendix, HamiltonÕs principle and Lagrange multiplier are used to derive the di¤erential-
algebraic equation for the sliderÐcrank mechanism. The motor-mechanism coupled system is shown in Fig. 2. The sliderÐcrank mechanism consists of three parts: crank, rod and slider. The positions of gravity centers of crank, rod and slider are, respectively,

$$x_{1cg} = 0, \qquad y_{1cg} = 0, \tag{A.1}$$

$$x_{2cg} = r\cos\theta + \frac{l\cos\phi}{2}, \quad y_{2cg} = \frac{l\sin\phi}{2}, \tag{A.2}$$

$$x_{3cg} = r\cos\theta + l\cos\phi + l', \quad y_{3cg} = 0. \tag{A.3}$$

The holomonic constraint equation [15] is

$$\Phi(\psi) = r\sin\theta - l\sin\phi = 0, \tag{A.4}$$

where $\psi = [\theta \ \phi]^{T}$ is the vector of generalized coordinates.

The kinematic velocity and acceleration equations are obtained by taking the Þrst and second derivatives of Eq. (A.4), respectively, as

$$\Phi_{\psi}\dot{\psi} = 0, \tag{A.5}$$

and

$$\Phi_{\psi}\ddot{\psi} = -(\Phi_{\psi}\dot{\psi})_{\psi}\dot{\psi} = \gamma, \tag{A.6}$$

where

$$\Phi_{\psi}\dot{\psi} = r\dot{\theta}\cos\theta - l\dot{\phi}\cos\phi, \tag{A.7}$$

$$\Phi_{\psi}\ddot{\psi} = r\dot{\theta}^{2}\sin\theta - l\dot{\phi}^{2}\sin\phi. \tag{A.8}$$

Total kinetic energy is

$$T = T_{1} + T_{2} + T_{3}, \tag{A.9}$$

where T_{1}, T_{2} and T_{3} represent the kinetic energies of crank, rod and slider, respectively,

$$T_{1} = \frac{1}{4}m_{1}R^{2}\dot{\theta}^{2}, \tag{A.10}$$

$$T_{2} = \frac{1}{6}m_{2}l^{2}\dot{\phi}^{2} + \frac{1}{2}m_{2}r^{2}\dot{\theta}^{2}\sin^{2}\theta + \frac{1}{2}m_{2}rl\dot{\theta}\dot{\phi}\sin\theta\sin\phi, \tag{A.11}$$

$$T_3 = \frac{1}{2}m_3 r^2 \dot{\theta}^2 \sin^2\theta + m_3 rl\dot{\theta}\dot{\phi}\sin\theta\sin\phi + \frac{1}{2}m_3 l^2\dot{\phi}^2 \sin^2\phi. \tag{A.12}$$

Let V_1 and V_2 represent the potential energies of crank and rod, respectively,

$$V_1 = 0, \tag{A.13}$$

$$V_2 = \frac{1}{2}m_2 gl\sin\phi. \tag{A.14}$$

The virtual work δW^A includes the applied torque τ with the virtual angle $\delta\theta$, the friction force F_B and the external force F_E with the virtual displacement δX_B. Thus, the following equation is obtained:

$$\delta W^A = \tau\delta\theta + (F_B - F_E)\delta X_B = \tau\delta\theta + F_{BE}(-r\sin\theta\delta\theta - l\sin\phi\delta\phi), \tag{A.15}$$

Where

$$F_B = -\mu m_3 g \, \text{sgn}(V_B),$$

$$\text{sgn}(V_B) = \begin{cases} 1 & \text{if} \quad V_B > 0, \\ 0 & \text{if} \quad V_B = 0, \\ -1 & \text{if} \quad V_B < 0. \end{cases}$$

and V_B is the velocity of the slider B.

Substituting Eq. (16) into Eq. (A.15) and rewriting in terms of the generalized coordinate ψ, then

$$\delta W^A = -\delta\psi^T Q^A,$$

where Q^A is the generalized force and given as

$$Q^A = \begin{bmatrix} F_{BE}r\sin\theta - n(K_t i_q^* - J_m\ddot{\theta}_r - B_m\dot{\theta}_r) \\ F_{BE}l\sin\phi \end{bmatrix}.$$

The generalized constraint reaction force can be obtained in term of Lagrange multiplier (Haug, 1992) as

$$Q^C = \Phi_\psi^T \lambda,$$

where λ is the Lagrange multiplier and

$$\Phi_\psi = [r\cos\theta \qquad -l\cos\phi]. \tag{A.16}$$

Thus, the virtual work by all constraint reaction forces is

$$\delta W^C = \delta\psi^T Q^C. \tag{A.17}$$

The general form of Hamilton's principle is

$$0 = \int_{t_1}^{t_2}[\delta L + \delta W^A + \delta W^C]dt$$

$$
= \int_{t_1}^{t_2} \delta\psi^{\mathrm{T}} \left[\frac{\partial L}{\partial \psi} - \frac{d}{dt}\left(\frac{\partial L}{\partial \dot{\psi}} \right) - Q^{A} + Q^{C} \right] dt, \tag{A.18}
$$

where L=T-V is called the Lagrangian [15], and $V = V_1 + V_2$.

The variational equations of Eq. (A.18) must hold for all $\delta\psi$. The varied path coincides with the true path at the two time ends t_1 and t_2. It follows that $\delta\psi(t_1) = \delta\psi(t_2) = 0$. Thus, the Euler Lagrange equations of motion, accounting for both applied and constraint forces, are

$$
M(\psi)\ddot{\psi} + N(\psi, \dot{\psi}) - BU - D(\psi) + \Phi_{\psi}^{\mathrm{T}}\lambda = 0, \tag{A.19}
$$

Where

$$
M(\psi) = \begin{bmatrix} -\dfrac{1}{2}m_1R^2 - (m_2 + m_3)r^2\sin^2\theta - n^2 J_m & -(\dfrac{1}{2}m_2 - m_3)r\,l\sin\theta\sin\phi \\[2ex] -(\dfrac{1}{2}m_2 - m_3)r\,l\sin\theta\sin\phi & -\dfrac{1}{3}m_2 l^2 - m_3 l^2\sin^2\phi \end{bmatrix},
$$

$$
N(\psi, \dot{\psi}) = \begin{bmatrix} -(m_2 + m_3)r^2\dot{\theta}^2\sin\theta\cos\theta - (\dfrac{1}{2}m_2 + m_3)r\,l\dot{\phi}^2\sin\theta\cos\phi - n^2 B_m\dot{\theta} \\[2ex] -(\dfrac{1}{2}m_2 + m_3)r\,l\dot{\theta}^2\cos\theta\sin\phi - m_3 l^2\dot{\phi}^2\sin\phi\cos\phi - \dfrac{1}{2}m_2 g l\cos\phi \end{bmatrix},
$$

$$
B = \begin{bmatrix} -nK_t \\ 0 \end{bmatrix}, \quad u = [I_q^*], \quad D(\psi) = \begin{bmatrix} F_{BE}\,r\sin\theta \\ F_{BE}\,l\sin\phi \end{bmatrix}
$$

58

Appendix B

Choose $v = [\theta]$, $u = [\phi]$, $\Phi_\upsilon = [r\cos\theta]$, and $\Phi_u = [-l\cos\phi]$. The entries of matrices in Eq. (15) are

$$M^{\upsilon\upsilon} = [-\frac{1}{2}m_1 R^2 - (m_2 + m_3)r^2 \sin^2\theta - n^2 J_m].$$

$$M^{\upsilon u} = [-(\frac{1}{2}m_2 - m_3)r l \sin\theta\sin\phi],$$

$$M^{u\upsilon} = [-(\frac{1}{2}m_2 - m_3)r l \sin\theta\sin\phi],$$

$$M^{uu} = [-\frac{1}{3}m_2 l^2 - m_3 l^2 \sin^2\phi],$$

$$N^\upsilon = [-(m_2 + m_3)r^2\dot{\theta}^2 \sin\theta\cos\theta - (\frac{1}{2}m_2 + m_3)r l \dot{\phi}^2 \sin\theta\cos\phi - n^2 B_m \dot{\theta}],$$

$$N^u = [-(\frac{1}{2}m_2 + m_3)r l \dot{\theta}^2 \cos\theta\sin\phi - m_3 l^2 \dot{\phi}^2 \sin\phi\cos\phi - \frac{1}{2}m_2 g l \cos\phi],$$

$$B^\upsilon = [-nK_t], \quad U = [i_q^*], \quad D^\upsilon = [F_{BE} r \sin\theta],$$

$$B^u = [0], \quad D^u = [F_{BE} l \sin\phi].$$

References

[1] Jasinski PW, Lee HC, Sandor GN. Vibrations of elastic connecting rod of a high-speed slider-crank mechanism.ASME Journal of Engineering for Industrial 1971;5:636-44.

[2] Zhu ZG, Chen Y. The stability of the motion of a connecting rod. ASME Journal of Mechanical Transmission, andAutomatic in Design 1983;105:637-40.

[3] Badlani M, Kleinhenz W. Dynamic stability of elastic mechanisms. ASME Journal of Mechanism Design1979;101:149-53.

[4] Viscomi BV, Arye RS.Nonlinear dynamic response of elastic slider-crank mechanism. ASME Journal of Engineeringfor Industrial 1971;93:251-62.

[5] Fung RF. Dynamic analysis of the flexible connecting rod of a slider-crank mechanism. ASME Journal of Vibrationand Acoustics 1996;118:687-9.

[6] Bose BK. Technology trends in microcomputer control of electrical machines. IEEE Transactions on IndustryElectronics 1988;35:160-76.

[7] Sen PC. Electric motor drives and control-past, present, and future. IEEE Transactions on Industry Electronics1990;37:562-75.

[8] Leonnard W. Microcomputer control of high dynamic performance ac drivesÐa survey. Automatica 1986;22:1-19.

[9] Utkin VI. Sliding mode in control and optimization. Berlin: Springer, 1992.

[10] Utkin VI. Sliding mode control design principles and applications to electric drives. IEEE Transactions on IndustryElectronics 1993;40:23-36.

[11] Yager RR, Filev DP. Essentials of fuzzy modeling and control. New York: Wiley, 1994.

[12] Krause PC. Analysis of electric machinery. New York: McGraw-Hill, 1986.

[13] Wehage RA, Haug EJ. Generalized coordinate partitioning for dimension reduction in analysis of constraineddynamic systems. ASME Journal of Mechanism Design, 1982;104:247Ð55.

[14] Slotine JJE, Li WP. Applied nonlinear control. Englewood Cliffs, New Jersey: Prentice-Hall, 1991.